Network Anomography

Yin Zhang
Dept. of Computer Science
University of Texas at Austin
Austin, TX 78712, USA
yzhang@cs.utexas.edu

Zihui Ge Albert Greenberg
AT&T Labs - Research
180 Park Avenue
Florham Park, NJ 07932, USA
{gezihui,albert}@research.att.com

Matthew Roughan
School of Mathematical Science
University of Adelaide
SA 5005, Australia
matthew.roughan@adelaide.edu.au

ABSTRACT

Anomaly detection is a first and important step needed to respond to unexpected problems and to assure high performance and security in IP networks. We introduce a framework and a powerful class of algorithms for *network anomography*, the problem of inferring network-level anomalies from widely available data aggregates. The framework contains novel algorithms, as well as a recently published approach based on Principal Component Analysis (PCA). Moreover, owing to its clear separation of inference and anomaly detection, the framework opens the door to the creation of whole families of new algorithms. We introduce several such algorithms here, based on ARIMA modeling, the Fourier transform, Wavelets, and Principal Component Analysis. We introduce a new *dynamic anomography* algorithm, which effectively tracks routing and traffic change, so as to alert with high fidelity on intrinsic changes in network-level traffic, yet not on internal routing changes. An additional benefit of dynamic anomography is that it is robust to missing data, an important operational reality. To the best of our knowledge, this is the first anomography algorithm that can handle routing changes and missing data. To evaluate these algorithms, we used several months of traffic data collected from the Abilene network and from a large Tier-1 ISP network. To compare performance, we use the methodology put forward earlier for the Abilene data set. The findings are encouraging. Among the new algorithms introduced here, we see: high accuracy in detection (few false negatives and few false positives), and high robustness (little performance degradation in the presence of measurement noise, missing data and routing changes).

1. INTRODUCTION

The first step in fixing a problem is knowing it exists. This is no less true in networking than anywhere else – we need to know about a problem before we can repair it. Networking vendors typically build alarms into network equipment to facilitate fast, accurate detection and diagnosis of problems. However, in practice, there are many problems for which explicit alarms are either absent (for new or uncommon problems), or intrinsically hard to produce. In these cases we must infer the problem from other data sources. For instance, many types of network problems cause abnormal patterns to appear in the network traffic. Such traffic *anomalies* may be caused by problems ranging from security threats such as Distributed Denial of Service (DDoS) attacks and network worms, to unusual traffic events such as flash crowds, to vendor implementation bugs, to network misconfigurations. We refer to the problem of inferring anomalies from indirect measurement as *network anomography* (combining "anomalous" with "tomography," a general approach to such inference problems).

Network tomography [37] bears some resemblance, in that both involve the solution of a linear inverse problem. Examples include inference of individual link performance characteristics from path performance characteristics, and inference of traffic matrices from individual link load measurements. For example, the traffic matrix estimation problem arises because the obvious source of data for direct measurement (flow-level data) can be hard to obtain network-wide [6, 16, 27, 29, 34, 37, 39, 40]. On the other hand, Simple Network Management Protocol (SNMP) data on individual link loads is available almost ubiquitously. Fortunately, the link loads and traffic matrices are simply related by a linear equation

$$\mathbf{b} = A\mathbf{x} \tag{1}$$

The vector $\mathbf{b}$ contains the link measurements, and A is the routing matrix (defined formally below). We wish to infer $\mathbf{x}$, which contains the unknown traffic matrix elements written as a vector. Tomographic inference techniques seek to invert this relationship to find $\mathbf{x}$.

The anomography problem is different and somewhat more complex. First, note that anomaly detection is performed on a series of measurements over a period of time, rather than from a single snapshot. In addition to changes in the traffic, the solution must build in the ability to deal with changes in routing. Second, note that the anomalies that we wish to infer may have dramatically different properties from a traffic matrix, and so different methods than those used for network tomography may be called for. Indeed, we find that simple extensions to network tomography methods perform fair poorly here. Techniques that transform the measurements prior to attempting to solve the inverse problem are preferable.

As a simple example, imagine trying to detect an anomalous traffic pattern caused by a flash crowd or DDoS attack on a web site. This type of event will cause increases in traffic flows headed towards a particular set of destinations. It may be hard to rapidly identify which of the tens of thousands of ingress links on a large network might be primarily responsible, as large surges at a network egress link may arise from small surges on several ingress links (ingress links can be large, multiplexing diverse and variable traffic). We must infer the change in the pattern of traffic to the particular site from the complete set of link data, considered together, rather than as individual time series. This illustrates an important feature of anomography – that it extends anomaly detection to network-level problems (automatically building in correlation across the network) where link-level anomaly detection might be inadequate or unreliable.

Many approaches to anomography are possible. In pioneering work, Lakhina *et al.* introduced a novel approach based on Principal Component Analysis (PCA) [23]. Our paper makes three major contributions to understanding and solving anomography problems:

1. We present a simple and powerful framework that encompasses a wide class of methods for network anomography. We will see that the method of [23] is a member of this class. The framework clearly decouples the inference and anomaly detection steps, and so immediately opens the door to the development of new algorithms where one makes different choices for each step. Accordingly, we introduce several such new algorithms here, based on ARIMA modeling,

the Fourier transform, Wavelets, and Principal Component Analysis. Moreover, the framework is not restricted to the analysis of link traffic data, and in particular also applies to the dual problem of inferring performance anomalies from end-to-end performance measurements.

2. We introduce a new algorithm for *dynamic anomography*, which identifies network level traffic anomalies and works in the presence of routing changes. That is, dynamic anomography tracks routing and traffic change – signaling traffic anomalies, but not internal network routing changes (which may dramatically change internal traffic patterns but may leave the traffic matrix, describing how traffic enters and exits the network, stable). In IP networks, routing changes occur as part of the normal "self-healing" behavior of the network, and so isolating these from traffic anomalies is advantageous. An additional benefit of dynamic anomography is that it is robust to missing link load measurements, an important operational reality (see Section 4 for why missing data may result in changes in the routing matrix). To the best of our knowledge, this is the first anomography algorithm that can handle routing changes and missing data.

3. Using data sets collected from a large Tier-1 ISP and from Internet2's Abilene network, we report on the results of an extensive and thorough evaluation of a set of anomography methods. To understand the fidelity of the methods and to compare different methods, we apply the methodology introduced in [23]. Under this methodology, we find that in general the new *temporal anomography* methods introduced here exhibit consistently high fidelity. In particular, we find that the most successful method (of those examined) is a variation of dynamic anomography, combining Box-Jenkins modeling (ARIMA) with ℓ^1 norm minimization. Further evaluation suggests that this algorithm can cope well with measurement noise, and degrade gracefully in the presence of missing or corrupted data.

The paper is organized as follows. Section 2 summarizes background and related work. In Section 3 we describe our framework, and the anomography algorithms examined in this paper, in the context of fixed routing. In Section 4 we extend the Box-Jenkins anomography to the case where routing may change over time. In Section 5 we describe our evaluation methodology, and Section 6 presents the results. Section 7 provides final remarks.

2. BACKGROUND

2.1 Network Tomography

Network tomography describes several problems: inferring topology, or link performance of a network from end-to-end measurements, or inferring Origin-Destination (OD) traffic demands from link traffic measurements. These problems can be written as linear inverse problems where one seeks to find unknowns $\mathbf{x}$ from measurements $\mathbf{b}$ given a linear relationship (1), where A is the routing matrix. For a network with n links, and m OD flows, we define the routing matrix to be the $n \times m$ matrix $A = [a_{ij}]$ where a_{ij} indicates the fraction of traffic from flow j to appear on link i.

Typically SNMP provides link measurements of traffic volumes (bytes and packets), typically at 5 minute intervals (this data is described in more detail in, for example [39]). We shall assume data of this type is the input to our algorithms, and we wish to infer anomalous traffic matrix elements, but note that anomography is not limited to this problem, and could equally be applied to inferring anomalous link performance from end-to-end measurements. An additional source of data used here comes from the routing protocols used to build the forwarding tables within each router. We use routing data (e.g., gathered from a route monitor as in [33]) along with a route simulator (as in [12]) to predict the results of these distributed computations, and determine the network routing.

The problem of inferring the OD traffic-matrix has been much studied recently (for examples see [6, 16, 27, 29, 34, 37, 39, 40]). The problem's key characteristic is that it is massively underconstrained: there will be approximately N^2 OD flows to estimate and only $O(N)$ link measurements. Hence tomography methods seek to introduce additional information, often in the form of some kind of traffic model (for instance a Poisson model in [37, 34], a Gaussian model in [6], or a gravity model in [39, 40]). Anomography problems are also highly underconstrained, but the models used to describe traffic are inappropriate for anomalies — by definition these events are generated by completely different processes from normal network traffic. Furthermore, in anomography we combine detection with inference, whereas in standard network tomography problems we seek only to infer a set of traffic matrix elements. Hence there are important differences between this paper and network tomography.

It is also important to note that routing matrices change over time. In much previous work, routing matrices are taken to be constant (an exception being [29], where the traffic is assumed to be somewhat constant, while the routing varies), but it is important (see [35]) to allow for the fact that routing is not constant, and neither is the traffic. In order to allow for variable routing, we index not just the traffic measurements over time, but also the routing matrix. Given these, we may write the relationship between the link traffic, and OD traffic matrix as

$$\mathbf{b}_j = A_j \mathbf{x}_j, \tag{2}$$

where A_j is an $n \times m$ routing matrix, $\mathbf{x}_j$ is a length-n vector of unknown OD flow traffic volumes, and $\mathbf{b}_j$ is a length-m vector of link loads[1], at time interval j.

2.2 Related work

Lakhina *et al.*carried out the pioneering work in the area of inference of anomalies at network level, [23, 22, 24], and adapted Principal Components Analysis (PCA) to this setting. Donoho [9, 10] introduced a powerful mathematical treatment for tomography-like problems, wherein one seeks solutions that maximize sparsity (intuitively, solutions with fewest explanations). These papers inspired our development of the new methods introduced here, and our development of a framework in which a very wide class of methods all fit.

Anomaly detection is a burgeoning field. A great deal of research in network anomaly detection relies on some type of inference step, taking a set of alarms [15, 17, 20, 31, 36] as input. While anomography includes methods of this type, our results indicate that it is better to delay alarm generation until after the inference step. In that way, a single constructive alarm may be generated, rather than a storm of redundant alarms. Moreover, in delaying the alarm generation until after the inference step, we can in some cases greatly improve the sensitivity of detection, as was demonstrated in [23].

We approach the network anomaly detection problem from the point of detecting unknown anomalous behavior, rather than looking for particular signatures in the data, the focus of much work in the security community. A large component of the work on machine learning, signal processing and time-series analysis is de-

[1]Note that the link load vector $\mathbf{b}_j$ also includes the aggregated traffic at different ingress/egress points; the corresponding rows in A_j encode the OD flows that enter/exit the network at these points.

voted to detecting outliers or anomalies in time-series. This literature has been applied to networks in a number of cases; for examples see [1, 5, 17, 21, 36, 38]. These methods range in sophistication from [5], which suggests the use of the standard Holt-Winters forecasting technique for network anomaly detection, to [1], which uses a sophisticated wavelet based method with great potential. These methods focus on single time series rather than the multi-dimensional time series that arise in anomography.

Most earlier work ignores noise or provides weak tests of robustness to noise (which can destroy utility). A strength of the work presented here is that we provide tests of effectiveness of the methods in the presence of noise, always a factor in practice.

3. NETWORK ANOMOGRAPHY

In this section, *we shall assume that the routing matrices A_j are time-invariant and are denoted by A.* (We will extend our work to time-varying A_j in Section 4.) Under this assumption, we can combine all t linear systems (2) into a single equation using matrix notation:

$$B = AX, \tag{3}$$

where $B = [\mathbf{b}_1\, \mathbf{b}_2 \cdots \mathbf{b}_t]$ is the matrix formed by having $\mathbf{b}_j$ as its column vectors, and similarly $X = [\mathbf{x}_1\, \mathbf{x}_2 \cdots \mathbf{x}_t]$.

3.1 A General Framework for Anomography

We identify two basic solution strategies to network anomography: (i) *early inverse*, and (ii) *late inverse*. Early-inverse approaches may appear more intuitive. The early-inverse approach tackles the problem in two steps. The first is the *network tomography* step, where OD flow data at each interval j are inferred from the link load measurements by solving the ill-posed linear inverse problem (2). Given the estimated OD flow data $\mathbf{x}_j$ at different time points j, in the second step, *anomaly detection* can then be applied to the $\mathbf{x}_j$. For this step, there are many widely used spatial and temporal analysis techniques, which we will describe later in this section.

Early-inverse methods, although conceptually simple, have an obvious drawback — errors in the first step, which are unavoidable due to the ill-posed nature of the inference problem, can contaminate the second step, sabotaging overall performance. Another disadvantage is that early-inverse methods apply a potentially computationally expensive anomaly detection step to high-dimensional data: on a network of N nodes, one must perform this step on all N^2 OD pairs. As we will see, late-inverse performs anomaly detection on only $O(N)$ dimensional data. We focus on late-inverse methods in this paper for these reasons, though we shall provide some comparisons between early- and late-inverse methods.

The idea of the late-inverse method is to defer "lossy" inference to the last step. Specifically, late inverse approaches extract the anomalous traffic from the link load observation, then form and solve a new set of inference problems:

$$\tilde{B} = A\tilde{X}, \tag{4}$$

where $\tilde{B} = [\tilde{\mathbf{b}}_1\, \tilde{\mathbf{b}}_2 \cdots \tilde{\mathbf{b}}_t]$ is the matrix of anomalous traffic in the observables, and $\tilde{X} = [\tilde{\mathbf{x}}_1\, \tilde{\mathbf{x}}_2 \cdots \tilde{\mathbf{x}}_t]$ is the matrix of OD flow anomalies to be diagnosed, over t time intervals.

While the new inference problems (4) share the same linear-inverse structure as in network tomography (3), the characteristics of the unknowns are very different, and so is the solution strategy, which we will explore in Section 3.4.

We now introduce a simple framework for late-inverse anomography methods. In this framework, $\tilde{B}$ is formed by multiplying B with a transformation matrix T. Depending on whether we use a left or right multiplying transformation matrix, we can further divide the framework into the following two classes:

- *spatial anomography*, where a left multiplying transformation matrix T is used to form $\tilde{B}$, *i.e.*, $\tilde{B} = TB$;
- *temporal anomography*, where a right multiplying transformation matrix T is used to form $\tilde{B}$, *i.e.*, $\tilde{B} = BT$.

As mentioned in Section 7, future work that might combine the best of spatial and temporal techniques would be of interest.

Our framework encompasses a number of analysis techniques for extracting anomalous traffic $\tilde{B}$ from link load observations B, as we next illustrate.

3.2 Spatial Anomography

Data elements in high dimensional data sets, such as the link load observations, usually have dependencies. The intrinsic dependency structure among the data elements can thus be exploited for filtering anomalous behavior by discovering data points that violate the normal dependency structure. In our context, the process of detecting such data points can be performed by left-multiplication by a transformation matrix T such that $\tilde{B} = TB$. An example of such an approach is a recent study by Lakhina *et al.* [23], where Principal Component Analysis (PCA) is used in finding dominant patterns. We describe this method, and in particular its instantiation as a left-multiplication operation in the following section.

3.2.1 Spatial PCA

In [23], Lakhina *et al.* proposed a subspace analysis of link traffic for anomaly detection, which can be summarized as follows.

1. Identify a coordinate transformation of B such that the link traffic data under the new coordinate systems have the greatest degree of variance along the first axis, the second greatest degree of variance along the second axis, and so forth. These axes are called the principal axes or principal components.
   Recall that $B = [\mathbf{b}_1\, \mathbf{b}_2 \cdots \mathbf{b}_t]$ is the collection of link traffic data at m links over t time intervals, where each row i ($1 \leq i \leq m$) denotes the time series of the i-th link and each column j ($1 \leq j \leq t$) represents an instance of all the link loads at time interval j. The principal components, $\mathbf{v}_1, \mathbf{v}_2, ..., \mathbf{v}_m$ can be computed iteratively as follows:
   $$\mathbf{v}_1 = \underset{\|\mathbf{v}\|=1}{\operatorname{argmax}} \left\| B^T\mathbf{v} \right\|,\ \mathbf{v}_k = \underset{\|\mathbf{v}\|=1}{\operatorname{argmax}} \left\| \left(B^T - \sum_{i=1}^{k-1} B^T\mathbf{v}_i\mathbf{v}_i^T \right)\mathbf{v} \right\|$$
   The coordinate transformation matrix can thus be obtained by arranging the principal components as rows of a matrix $P = [\mathbf{v}_1\, \mathbf{v}_2 ... \mathbf{v}_m]^T$.
2. Divide the link traffic space into the *normal subspace* and the *anomalous subspace*. Lakhina *et al.* [23] developed a threshold-based separation method by examining the projection of the time series of link traffic data on each principal axis in order. As soon as a projection is found that contains a 3σ deviation from the mean, that principal axis and all subsequent axes are assigned to the anomalous subspace. All previous principal axis are assigned to the normal subspace.
   We use $P_a = [\mathbf{v}_r\, \mathbf{v}_{r+1} ... \mathbf{v}_m]^T$ to denote the matrix of the principal axes in the anomalous subspace, where $\mathbf{v}_r$ is the first axis that fails to pass the threshold test.
3. The anomalous traffic can now by extracted from link load observation by first projecting the data into the anomalous subspace and then transforming it back, by taking $\tilde{B} = (P_a^T P_a)B$, and so we obtain the transformation matrix $T = P_a^T P_a$.

We call the above method *spatial PCA* because it exploits the correlation between traffic on different links (across space). Later in Section 3.3.4, we will describe *temporal PCA*, which exploits temporal correlation by applying PCA to identify dominant patterns across time.

3.3 Temporal Anomography

The anomalous link traffic can also be separated by performing temporal analysis on the time series for each link. Consider a set of link traffic data over time t: $B = [\mathbf{b}_1\, \mathbf{b}_2 ... \mathbf{b}_t]$. The process of extracting anomalies by exploiting the temporal structure within the data points can be modeled as a linear transformation of the time series: $\tilde{B} = [\tilde{\mathbf{b}}_1\, \tilde{\mathbf{b}}_2 ... \tilde{\mathbf{b}}_t] = BT$, where the transformation matrix T can be either explicit or implicit. In this paper, we consider four types of temporal analysis: ARIMA, Fourier, Wavelet, and PCA (for identifying dominant patterns across time). Although it may not be obvious at first glance, all these methods indeed fit in our framework of linear matrix transformation, as we will see next.

3.3.1 ARIMA Modeling

Univariate time series. The Box-Jenkins methodology, or AutoRegressive Integrated Moving Average (ARIMA) modeling technique [2, 3, 4], is a class of linear time-series forecasting techniques that capture the linear dependency of the future values on the past. It is able to model a wide spectrum of time-series behavior, and has been extensively used for anomaly detection in univariate time-series.

An ARIMA model includes three order parameters: the autoregressive parameter (p), the number of differencing passes (d), and the moving average parameter (q). In the notation introduced by Box and Jenkins, models are summarized as ARIMA(p, d, q). A model described as ARIMA$(0, 1, 2)$ means that it contains $p = 0$ (zero) autoregressive parameters and $q = 2$ moving-average parameters which were computed for the time series after it was differenced once ($d = 1$).

A general ARIMA model of order (p, d, q) can be expressed as:

$$z_k - \sum_{i=1}^{p} \phi_i \cdot z_{k-i} = e_k - \sum_{j=1}^{q} \theta_j \cdot e_{k-i}, \tag{5}$$

where z_k is obtained by differencing the original time series d times (when $d \geq 1$) or by subtracting the mean from the original time series (when $d = 0$), e_k is the forecast error at time k, ϕ_i ($i = 1, ..., p$) and θ_j ($j = 1, ..., q$) are the autoregression and moving-average coefficients, respectively.

Many commonly used smoothing models are special instances of ARIMA models. For example, the Exponentially Weighted Moving Average (EWMA), is equivalent to ARIMA$(0, 1, 1)$; linear exponential smoothing, also known as non-seasonal Holt-Winters, is equivalent to ARIMA$(0, 2, 2)$. These techniques have been used for detecting anomalies in time-series, for instance Hood and Ji [17] use an ARIMA$(0, 0, 2)$ model. See [32] for detailed equations for various smoothing models and their equivalence with ARIMA models.

There are well known techniques for estimating the parameters p, d, q, ϕ_i and θ_j for a given time series [2, 3, 4], and given the parameters, the model is simply applied to get $\hat{z}_k$ a prediction of z_k (using for instance the Durbin-Levinson algorithm [4]). The prediction errors are then $e_{k+1} = z_{k+1} - \hat{z}_{k+1}$, which then form our anomalous traffic (the traffic which does not fit the model). In practice the parameters used in the ARIMA model are sometimes chosen to meet particular goals intended by the implementor (see [5] for some discussion of these choices), rather than being estimated from the data set, because the parameters of a data set may change over time. However, we prefer to use adaptive techniques to overcome this problem.

If we consider the time series to be vectors of length t, then the above results can be written in matrix form. Taking the measurements $\mathbf{b} = (b_1, \ldots, b_t)^T$, we can obtain the errors $\mathbf{e} = (e_1, \ldots, e_t)^T$, via right-multiplication by a transformation matrix $\tilde{\mathbf{b}}^T = \mathbf{e}^T = \mathbf{b}^T T$. Specifically, let I denote the $t \times t$ identity matrix, $\bigtriangledown$ denote the "back shift" matrix, and $\mathbf{1}$ denote the $t \times t$ unit matrix, i.e.,

$$I = \begin{bmatrix} 1\,0\,0 ... 0\,0 \\ 0\,1\,0 ... 0\,0 \\ \cdots \\ 0\,0\,0 ... 1\,0 \\ 0\,0\,0 ... 0\,1 \end{bmatrix},\ \bigtriangledown = \begin{bmatrix} 0\,1\,0 ... 0\,0 \\ 0\,0\,1 ... 0\,0 \\ \cdots \\ 0\,0\,0 ... 0\,1 \\ 0\,0\,0 ... 0\,0 \end{bmatrix},\ \mathbf{1} = \begin{bmatrix} 1\,1\,1 ... 1\,1 \\ 1\,1\,1 ... 1\,1 \\ \cdots \\ 1\,1\,1 ... 1\,1 \\ 1\,1\,1 ... 1\,1 \end{bmatrix}.$$

The differencing result, $\mathbf{z} = [z_1 z_2 ... z_t]^T$, can then be represented by

$$\mathbf{z}^T = \begin{cases} \mathbf{b}^T (I - \bigtriangledown)^d, & \text{for } d \geq 1, \\ \mathbf{b}^T - \frac{1}{t}\mathbf{b}^T \mathbf{1} = \mathbf{b}^T \left(I - \frac{1}{t}\mathbf{1} \right), & \text{for } d = 0, \end{cases} \tag{6}$$

Equation (5) can be written in matrix notation as

$$\mathbf{z}^T - \sum_{i=1}^{p} \phi_i \mathbf{z}^T \bigtriangledown^i = \mathbf{e}^T - \sum_{j=1}^{q} \theta_j \mathbf{e}^T \bigtriangledown^j,$$

or equivalently,

$$\mathbf{e}^T = \mathbf{z}^T \left(I - \sum_{i=1}^{p} \phi_i \bigtriangledown^i \right) \left(I - \sum_{j=1}^{q} \theta_j \bigtriangledown^j \right)^{-1}.$$

Extending ARIMA based models to multivariate time series is straightforward. As noted earlier, we construct the matrix B with the measurements at each time period $\mathbf{b}_i$ as its columns. Via the transformations just described, we obtain

$$E = Z \left(I - \sum_{i=1}^{p} \phi_i \bigtriangledown^i \right) \left(I - \sum_{j=1}^{q} \theta_j \bigtriangledown^j \right)^{-1}. \tag{7}$$

ARIMA based anomography. Replacing Z by the matrix form of (6), we see that $E = BT$ is indeed a transformation given by right-multiplying B with a matrix T. In fact, any *linear* filtration of the elements of a time series can be modeled by a right multiplying matrix transformation. If the transformation is time-invariant, then the matrix in question will be Toeplitz (the values along diagonals will be constant).

To get back to anomaly detection, we simply identify the forecast errors as anomalous link traffic, $\tilde{B} = E$. That is, traffic behavior that cannot be well captured by the model is considered anomalous.

3.3.2 Fourier Analysis

Fourier analysis [26] is the process of decomposing a complex periodic waveform into a set of sinusoids with different amplitudes, frequencies and phases. The sum of these sinusoids can exactly match the original waveform. This lossless transform presents a new perspective of the signal under study (in the frequency domain), which has proved useful in very many applications.

For a discrete-time signal $x_0, x_1, \ldots, x_{N-1}$, the Discrete Fourier Transform (DFT) is defined by

$$f_n = \frac{1}{N} \sum_{k=0}^{N-1} x_k e^{-jk2\pi n/N}, \quad \text{for } 0 \leq n \leq N-1,$$

where f_n is a complex number that captures the amplitude and phase of the signal at the n-th harmonic frequency (with base frequency $1/N$). Note that for a real signal $\{f_n\}$ is symmetric, i.e., $f_n = f_{N-1-n}$. Lower n corresponds to a lower frequency component, with f_0 being the DC component, or the average of the input series, and f_n with n close to $N/2$ corresponding to high frequencies.

The Inverse Discrete Fourier Transform (IDFT) is used to reconstruct the signal in the time domain by

$$x_n = \sum_{k=0}^{N-1} f_k e^{jk2\pi n/N}, \quad \text{for } 0 \le n \le N-1.$$

An efficient way to implement the DFT and IDFT is through an algorithm called the Fast Fourier Transform (FFT). The computational complexity of the FFT is $O(N \log(N))$.

FFT based anomography. The idea of using the FFT to extract anomalous link traffic, $\tilde{B}$ is to filter out the low frequency components in the link traffic time series. In general, low frequency components capture the daily and weekly traffic patterns, while high frequency components represent the sudden changes in traffic behavior. Working in the frequency domain provides us with the opportunity to distinguish these two kinds of behaviors.

We summarize FFT based anomography as follows.

1. Transform link traffic B into the frequency domain: $F = \text{FFT}(B)$: apply the FFT on each row of B. (Recall that a row corresponds to the time series of traffic data on one link.) The result is the corresponding frequency domain series, in each row of F.
2. Remove low frequency components: i.e. set $F_i = 0$, for $i \in [1, c] \cup [N-c, N]$, where F_i is the i-th column of F and c is a cut-off frequency. (For example, for the results presented in Section 6, we use 10-minute aggregated link traffic data of one week duration, and $c = \lceil \frac{10}{60} N \rceil$, corresponding to a frequency of one cycle per hour.)
3. Transform back into the time domain: i.e. we take $\tilde{B} = \text{IFFT}(F)$. The result is the high frequency components in the traffic data, which we will use as anomalous link traffic, $\tilde{B}$.

The DFT and IDFT may be represented as right-matrix products. In setting columns of F to zero, and performing the IDFT we are taking a linear combination of the columns of F, which in turn are a linear combination of those of B. Hence, the overall process above can be modeled as a right-multiplying matrix transformation $\tilde{B} = BT$. Note also that in thresholding at frequency c we preserve the symmetry of F, and so although F may contain complex elements, the resulting transform will be real.

3.3.3 Wavelet Analysis

Wavelets [8, 14, 26] are mathematical functions that cut up data into different frequency components, and then study each component with a resolution matched to its scale. They provide a powerful means for isolating characteristics of signals via a combined time-frequency representation and are often considered superior to traditional Fourier methods especially in situations where the signal contains transients, such as discontinuities and sharp spikes.

In [1], Barford *et al.* have developed a wavelet-based algorithm for detecting anomalies in the link traffic data. It shares the same principle as the FFT based approaches — exposing anomalies by filtering low frequency components. More specifically, it uses wavelets to decompose the original signal into low-, mid-, and high-frequency components and then detects anomalies by close examination of the mid- and high-frequency components.

Below we compute $\tilde{B}$ as the high-frequency components of link traffic B. We can also compute $\tilde{B}$ as the mid-frequency components of B in essentially the same way.

1. Use wavelets to decompose B into different frequency levels: $W = \text{WAVEDEC}(B)$, by applying a multi-level 1-D wavelet decomposition on each row of B. The result is a wavelet decomposition vector, which we save as one row in matrix W. The wavelet we use is the Daubechies wavelet [7] of order 6.
2. Then remove low- and mid-frequency components in W by setting all coefficients at frequency levels higher than w_c to 0. Here w_c is a cut-off frequency level. For the results presented in Section 6, we use 10-minute aggregated link traffic data of one week duration, and w_c is set at 3. That is, we only keep coefficients at frequency levels 1, 2, and 3, which is consistent with [1].
3. Reconstruct the signal: $\tilde{B} = \text{WAVEREC}(B)$. The result is the high-frequency components in the traffic data.

It is easy to verify that the process of WAVEDEC and WAVEREC only involves linear combinations of columns of B. As a result, the $\tilde{B}$ derived through the wavelet based anomography can also be modeled as right multiplying matrix transformation.

3.3.4 Temporal PCA

In Section 3.2.1, we presented a method of applying PCA to find dominant patterns among different link-load time series. A similar method can be used in identifying dominant patterns across time.

Consider the link load matrix $B = [\mathbf{b}_1\, \mathbf{b}_2 ... \mathbf{b}_t]$. We can think of each row as a t-dimensional vector. What we are looking for is a new coordinate system, $\mathbf{v}_1$, $\mathbf{v}_2$, ... ,$\mathbf{v}_t$, such that the projection of the m links (on $\mathbf{v}_1$, $\mathbf{v}_2$, ..., $\mathbf{v}_t$) has energy concentrated on the first several axes. This is exactly what PCA provides. The only difference is that we now apply PCA on B^T as opposed to B (as used in spatial PCA). Then we follow the same procedure to define an anomalous subspace and to extract anomalies that have projections in the anomalous subspace. In this way, we obtain a left multiplying transformation matrix T, i.e., $\tilde{B}^T = TB^T$. Taking transpose on both side of the equation, we have $\tilde{B} = (\tilde{B}^T)^T = (TB^T)^T = BT^T$ where T^T is a right multiplying transformation matrix that extracts anomalies from B.

3.4 Inference algorithms

Once we obtain the matrix of link anomalies $\tilde{B}$, the next step is to reconstruct OD flow anomalies $\tilde{X}$ by solving a series of ill-posed linear inverse problems $\tilde{\mathbf{b}}_j = A\tilde{\mathbf{x}}_j$. For example, Lakhina *et al* [23] proposed to find the single largest anomaly in each time interval j by applying a greedy algorithm. We present below three common inference algorithms for solving these problems. All three algorithms deal with the underconstrained linear system by searching for a solution that minimizes some notions of vector norm, three examples of which are

- The ℓ^2 norm of a vector $\mathbf{v}$ is defined as $\|\mathbf{v}\|_2 = \left(\sum_i v_i^2\right)^{\frac{1}{2}}$, where v_i is the i-th element of vector $\mathbf{v}$.
- The ℓ^1 norm of a vector $\mathbf{v}$ is defined as $\|\mathbf{v}\|_1 = \sum_i |v_i|$, *i.e.*, the sum of the absolute value of each element of $\mathbf{v}$.
- The ℓ^0 norm of a vector $\mathbf{v}$ is defined as $\|\mathbf{v}\|_0 = \sum_i v_i^0$, *i.e.*, the number of non-zero elements of $\mathbf{v}$.

3.4.1 Pseudoinverse solution

A standard solution to $\tilde{\mathbf{b}} = A\tilde{\mathbf{x}}$ is the pseudoinverse solution $\tilde{\mathbf{x}} = A^+\tilde{\mathbf{b}}$, where A^+ is the pseudoinverse (or Moore-Penrose inverse) of matrix A. It is known that $\tilde{\mathbf{x}} = A^+\tilde{\mathbf{b}}$ is the solution to

the problem $\tilde{\mathbf{b}} = A\tilde{\mathbf{x}}$ that minimizes the ℓ^2 norm of the anomaly vector, i.e. it solves:

$$\text{minimize } \|\tilde{\mathbf{x}}\|_2 \quad \text{subject to } \|\tilde{\mathbf{b}} - A\tilde{\mathbf{x}}\|_2 \text{ is minimal.} \tag{8}$$

3.4.2 Sparsity maximization

In practice, we expect only a few anomalies at any one time, so $\tilde{\mathbf{x}}$ typically has only a small number of large values. Hence it is natural to proceed by maximizing the *sparsity* of $\tilde{\mathbf{x}}$, *i.e.*, solving the following ℓ^0 norm minimization problem:

$$\text{minimize } \|\tilde{\mathbf{x}}\|_0 \quad \text{subject to } \tilde{\mathbf{b}} = A\tilde{\mathbf{x}}. \tag{9}$$

The ℓ^0 norm is not convex and is notoriously difficult to minimize, so in practice one needs to either approximate the ℓ^0 norm with a convex function or use heuristics, for example the greedy algorithm of Lakhina *et al* [23].

3.4.2.1 ℓ^1 norm minimization.

One common approach to approximate ℓ^0 norm minimization is to convexify (9) by replacing the ℓ^0 norm with an ℓ^1 norm, so that we seek a solution to

$$\text{minimize } \|\tilde{\mathbf{x}}\|_1 \quad \text{subject to } \tilde{\mathbf{b}} = A\tilde{\mathbf{x}} \tag{10}$$

As shown in [9, 10], ℓ^1 norm minimization results in the sparsest solution for many large under-determined linear systems.

In the presence of measurement noise, the constraints $\tilde{\mathbf{b}} = A\tilde{\mathbf{x}}$ may not always be satisfiable. In this case, we can add a penalty term $\|\tilde{\mathbf{b}} - A\tilde{\mathbf{x}}\|_1$ to the objective and reformulate (10) as:

$$\text{minimize} \quad \lambda\|\tilde{\mathbf{x}}\|_1 + \|\tilde{\mathbf{b}} - A\tilde{\mathbf{x}}\|_1 \tag{11}$$

where $\lambda \in [0, 1]$ controls the degree to which the constraints $\tilde{\mathbf{b}} = A\tilde{\mathbf{x}}$ are satisfied. As shown in Section 6, the algorithm is not very sensitive to the choice of λ. In the rest of this paper, unless noted otherwise, we use $\lambda = 0.001$, which gives satisfactory results.

We can cast (11) into the following equivalent Linear Programming (LP) problem, for which solutions are available even when A is very large, owing to modern interior-point linear programming methods.

$$\begin{array}{ll} \text{minimize} & \lambda \sum_i u_i + \sum_j v_j \\ \text{subject to} & \tilde{\mathbf{b}} = A\tilde{\mathbf{x}} + \mathbf{z} \\ & \mathbf{u} \geq \tilde{\mathbf{x}}, \quad \mathbf{u} \geq -\tilde{\mathbf{x}} \\ & \mathbf{v} \geq \mathbf{z}, \quad \mathbf{v} \geq -\mathbf{z} \end{array} \tag{12}$$

Note that it is common to use $\|\tilde{\mathbf{b}} - A\tilde{\mathbf{x}}\|_2^2$ (instead of $\|\tilde{\mathbf{b}} - A\tilde{\mathbf{x}}\|_1$) as the penalty term in (11). This alternative formulation can be efficiently solved using methods like Iterative Reweighted Least Squares [19] and has been successfully applied in [11] to recover sparse overcomplete representations in the presence of noise. We elect to use (11) because we find it much easier to generalize (11) to detect changes when the routing matrix A is time varying (see Section 4 for details).

3.4.2.2 Greedy algorithm.

Another common heuristic solution for ℓ^0 norm minimization is to apply the greedy algorithm. For example, the greedy heuristic has been successfully applied to wavelet decomposition, where it goes by the name of *Orthogonal Matching Pursuit* (OMP) [30]. In the same spirit here, we develop a greedy solution to maximize the sparsity of $\tilde{\mathbf{x}}$. The algorithm starts with an empty set I of non-zero positions for $\tilde{\mathbf{x}}$ and then iteratively adds new non-zero positions to I. During each iteration, for each position $p \notin I$, the algorithm tests how much it can reduce the residual $\tilde{\mathbf{b}} - A\tilde{\mathbf{x}}$ by including p as a non-zero position. More specifically, let $J = I \cup \{p\}$. The algorithm estimates the values for the non-zero elements of $\tilde{\mathbf{x}}$ (denoted as $\tilde{\mathbf{x}}_J$) by solving the following least squares problem

$$\text{minimize } \|\tilde{\mathbf{b}} - A_J\tilde{\mathbf{x}}_J\|_2 \tag{13}$$

where $A_J = A[., J]$ is a submatrix of A formed by the column vectors of A corresponding to positions in J. The residual is then computed as $e_J = \|\tilde{\mathbf{b}} - A_J\tilde{\mathbf{x}}_J\|_2$. The algorithm then greedily chooses the position p that gives the smallest e_J and adds it to I. The algorithm stops whenever either the residual energy falls below some tolerance to inaccuracy $e_{\max}$ or the number of non-zero positions exceeds some threshold $\ell^0_{\max}$.

4. DYNAMIC NETWORK ANOMOGRAPHY

Up to this point, we have assumed that the routing matrices are constant. However, we wish to allow for dynamic routing changes, and so we must allow A_j to vary over time. In IP networks, routing changes occur as part of the normal "self-healing" behavior of the network, and so it is advantageous to isolate these from traffic anomalies and only signal traffic anomalies. In addition, if some measurements are missing (say at time j), we may still form a consistent problem by setting the appropriate rows of A_j to zero. Thus, for realistic SNMP measurements where missing data are often an issue, we still wish to vary A_j even for static routing. Routing measurements may be obtained using a route monitor, to provide accurate, up-to-date measurements of routing (at least at the time scale of SNMP measurements, e.g. minutes).

Where the tomography step can be done separately at each time interval (for instance see [39, 40]), it is simple to adapt early-inverse methods to *dynamic network anomography* by inverting (2) at each time step. Given the straight forward approach for early-inverse methods, We seek here to generalize late-inverse methods to dynamic network anomography.

4.1 Dynamic temporal anomography

When the routing matrix is non-constant, there is no reason to believe that the measurements B should follow a simple model such as an ARIMA model. Even where the traffic itself follows such a model, a simple routing change may change a link load measurement by 100%, for instance by routing traffic completely away from a particular link. If we were to apply the ARIMA model to the measurements B, we would see such a change in routing as a level-shift anomaly. However, its cause is not an unknown change in X (to be discovered), but rather a known change in the routing matrices A_j. Likewise, it no longer makes sense to try to exploit spatial correlations which arose from a particular routing, to the case of another routing.

However, it is no less reasonable to approximate the traffic matrix X by an ARIMA model (than B when the routing is constant), even when routing may change. Under such a modeling assumption, we can write $\tilde{X} = XT$. We know also that the measurements are given by (2). A reasonable approach to the solution is therefore to seek a solution $\tilde{X}$ which is consistent with these equations, but also minimizes one of the norms (described above) at each time step. We choose to minimize the ℓ^1 norm $\|\tilde{\mathbf{x}}_j\|_1$ here because (i) it allows us to naturally incorporate link load constraints at multiple time intervals, and (ii) it is more accurate than both the pseudoinverse and the greedy algorithms for static anomography (as we will show in Section 6).

Unfortunately, for transform based methods (the Fourier, wavelet and PCA methods) the number of constraints becomes very large (as t grows). On the other hand, the set of constraints for the ARIMA model can be written in a form such that it does not grow

with t. Hence, in the following we concentrate on generalizing the ARIMA approach. We first present the basic algorithm for ARIMA(p, d, q) models with $d \geq 1$ (Section 4.2). To improve its efficiency, we develop two simple techniques that significantly reduce the problem size (Section 4.3). We have also extended the algorithm to handle ARIMA models with $d = 0$ (Section 4.4). We will also discuss model selection and parameter estimation, two important issues for applying ARIMA-based anomography (Section 4.5).

4.2 Algorithm for ARIMA models with $d \geq 1$

We are going to seek solutions that are consistent with the measurements $\mathbf{b}_j = A_j\mathbf{x}_j$, for $j = 1, \ldots, t$, and an ARIMA model that gives $\tilde{X} = XT$ where T is the same transformation matrix implicitly defined by (6) and (7). Importantly, we do not wish to have to estimate X (or we may as well use an early-inverse method). The advantage of the ARIMA model, is we do not need to know X, but only linear combinations of X.

Let L be the backshift operator, whose effect on a process $\mathbf{z}$ can be summarized as $(L\mathbf{z})_k = \mathbf{z}_{k-1}$. Let the AR polynomial $\Phi(L)$ be

$$\Phi(L) = \sum_{i=0}^{d+p} \gamma_i L^i \stackrel{\text{def}}{=} \left(1 - \sum_{i=1}^{p} \phi_i L^i\right)(1-L)^d.$$

Let $\mathbf{y}_{k-i} = \gamma_i \mathbf{x}_{k-i}$. We now identify $\mathbf{e} = \tilde{\mathbf{x}}$ in the ARIMA model described in (5) (or rather its multivariate extension). By definition the sum $\sum_{i=0}^{d+p} \mathbf{y}_{k-i} = \mathbf{z}_k - \sum_{i=1}^{p} \phi_i \mathbf{z}_{k-i}$, and so, for $d \geq 1$, the ARIMA model (5) can be rewritten

$$\sum_{i=0}^{d+p} \mathbf{y}_{k-i} = \tilde{\mathbf{x}}_k - \sum_{j=1}^{q} \theta_j \tilde{\mathbf{x}}_{k-j}. \tag{14}$$

Define $\mathbf{c}_{k-i} = \gamma_i \mathbf{b}_{k-i}$, then as $\mathbf{y}_{k-i} = \gamma_i \mathbf{x}_{k-i}$, the measurement equation (2) implies

$$A_{k-i}\mathbf{y}_{k-i} = \mathbf{c}_{k-i}, \quad i = 0, 1, \cdots, d+p. \tag{15}$$

We can compute $\tilde{\mathbf{x}}_1, \tilde{\mathbf{x}}_2, \cdots, \tilde{\mathbf{x}}_t$ iteratively by solving a series of ℓ^1 norm minimization problems $\mathcal{P}_k$ ($k = 1, 2, \cdots, t$):

$$\mathcal{P}_k: \quad \text{minimize } \|\tilde{\mathbf{x}}_k\|_1 \text{ subject to (14) and (15).} \tag{16}$$

As an illustrative example, consider the simplest ARIMA model, ARIMA$(0, 1, 0)$. In this case, $p = q = 0$, so we can write

$$\Phi(L) = \sum_{i=0}^{1} \gamma_i L^i = (1 - L),$$

so $\gamma_0 = 1$ and $\gamma_1 = -1$, and (14) becomes $\tilde{\mathbf{x}}_k = \sum_{i=0}^{1} \mathbf{y}_{k-i}$, thus problem $\mathcal{P}_k$ is simply

$$\begin{array}{ll} \text{minimize} & \|\tilde{\mathbf{x}}_k\|_1 \\ \text{subject to} & \left\{ \begin{array}{rcl} \tilde{\mathbf{x}}_k & = & \mathbf{y}_k + \mathbf{y}_{k-1} \\ A_k\mathbf{y}_k & = & \mathbf{b}_k \\ A_{k-1}\mathbf{y}_{k-1} & = & -\mathbf{b}_{k-1} \end{array} \right. \end{array} \tag{17}$$

We apply zero-padding to handle the initial condition when $k \leq q$ or $k \leq d + p$. Specifically, for the MA part of the model, we set $\tilde{\mathbf{x}}_{k-j}$ to 0 whenever $k \leq j$. For the AR part of the model, we apply zero-padding on the differenced series $\{(1-L)^d\mathbf{x}_i\}$, which can be achieved by redefining the AR polynomial $\Phi(L) = \sum_i \gamma_i L^i$ as

$$\Phi(L) \stackrel{\text{def}}{=} \left\{ \begin{array}{ll} (1 - \sum_{i=1}^{p} \phi_i L^i)(1-L)^d & \forall k > d + p \\ (1 - \sum_{i=1}^{k-d} \phi_i L^i)(1-L)^d & \forall k \in (d, d+p] \\ 0 & \forall k \leq d \end{array} \right.$$

As in Section 3.4.2.1, we can accommodate measurement noise by incorporating penalty terms into the objective to penalize against violation of constraints (14) and (15). We can then solve the resulting ℓ^1 norm minimization problem by reformulating it as an equivalent LP problem. We omit such details in the interest of brevity.

4.3 Reducing the problem size

One potential problem with the above algorithm is its high computational cost. Even though the computational cost is fixed relative to t, it is still highly dependent on the number of traffic matrix elements n, and the order parameters (p, d, q), and so the ℓ^1 minimization problem $\mathcal{P}_k$ can be very large even when A_{k-i} stays constant. In contrast, the static anomography algorithm had quite good computation properties for constant A_j. Below we develop two simple techniques to significantly reduce the size of $\mathcal{P}_k$. These techniques are motivated by the following observations: (i) the routing matrices are often quite stable and tend not to change in every time interval; and (ii) when the changes occur, they tend to be local changes and most rows of the routing matrix will remain the same. Our techniques seek to merge constraints if the corresponding link load is unaffected by the change of the routing matrix. In particular, for time invariant A_j, our techniques reduce the dynamic anomography to the static anomography algorithm.

Eliminating duplicate A_{k-i}. Our first technique reduces the problem size by merging constraints for intervals with the same routing matrix. Specifically, if there exist $i_1 < i_2$ such that $A_{k-i_1} = A_{k-i_2}$, we can use a single unknown vector $\mathbf{y}'_{k-i_1}$ to represent $\mathbf{y}_{k-i_1} + \mathbf{y}_{k-i_2}$ in (14) and then replace the two sets of constraints on $\mathbf{y}_{k-i_1}$ and $\mathbf{y}_{k-i_2}$ in (15) with a single set of constraints on $\mathbf{y}'_{k-i_1}$:

$$A_{k-i_1}\mathbf{y}'_{k-i_1} = \mathbf{c}'_{k-i_1} \stackrel{\text{def}}{=} \mathbf{c}_{k-i_1} + \mathbf{c}_{k-i_2}$$

We can repeat this process until all A_{k-i} are distinct.

Eliminating rows common to all A_{k-i}. Our second technique exploits the fact that there is often a large subset of rows common to all A_{k-i}. Before describing the technique, we first introduce some notations. Let S be a set of integers. Given a matrix M, let M^S be the submatrix of M that consists of all rows with indices in S. Similarly, given a vector $\mathbf{v}$, let $\mathbf{v}^S$ be the subvector of $\mathbf{v}$ that consists of elements with indices in S.

Using the above notations, let C be the set of row indices such that all A^C_{k-i} are equal (denoted by A^C). Let $\overline{C}$ be the set of row indices not in C. We can then decompose (15) into

$$A^C\mathbf{y}_{k-i} = \mathbf{c}^C_{k-i}, \quad i = 0, 1, \cdots, d+p \tag{18}$$

$$A^{\overline{C}}_{k-i}\mathbf{y}_{k-i} = \mathbf{c}^{\overline{C}}_{k-i}, \quad i = 0, 1, \cdots, d+p \tag{19}$$

Summing up all the constraints in (18) over i, we obtain

$$A^C \sum_{i=0}^{d+p} \mathbf{y}_{k-i} = \sum_{i=0}^{d+p} \mathbf{c}^C_{k-i} \tag{20}$$

Combining (20) and (14), we get a single set of constraints on $\tilde{\mathbf{x}}_k$:

$$\sum_{i=0}^{d+p} \mathbf{c}^C_{k-i} = A^C\tilde{\mathbf{x}}_k - A^C \sum_{j=1}^{q} \theta_j \tilde{\mathbf{x}}_{k-j} \tag{21}$$

We can then replace (18) with (21), reducing $\mathcal{P}_k$ to

$$\text{minimize } \|\tilde{\mathbf{x}}_k\|_1 \text{ subject to (14), (19), and (21).} \tag{22}$$

In the special case when A_j is time invariant, we have $\overline{C} = \emptyset$. So the constraints on $\mathbf{y}_{k-i}$ (19) become empty, causing $\mathbf{y}_{k-i}$ to

become free variables in (22). In this case, we can further simplify (22) by eliminating $\mathbf{y}_{k-i}$ and the corresponding constraint (14), resulting in

$$\text{minimize } \|\tilde{\mathbf{x}}_k\|_1 \text{ subject to (21).} \tag{23}$$

It is easy to verify that (23) is equivalent to our original algorithm for time invariant A_j, which first computes $\tilde{B}$ by applying ARIMA modeling on B and then estimates $\tilde{\mathbf{x}}_k$ by minimizing $\|\tilde{\mathbf{x}}_k\|_1$ subject to $\tilde{\mathbf{b}}_k = A\tilde{\mathbf{x}}_k$. This is appealing in that we now have one unified algorithm for ARIMA-based anomography.

4.4 Algorithms for ARIMA models with $d = 0$

We now extend the algorithm to deal with ARIMA(p, d, q) models with $d = 0$. The main difference from ARIMA models with $d \geq 1$ is that we need to subtract the mean of process $\{\mathbf{x}_t\}$ (denoted by μ) from $\mathbf{x}_t$ in the analysis. That is, we have

$$(\mathbf{x}_k - \mu) - \sum_{i=1}^{p} \phi_i(\mathbf{x}_{k-i} - \mu) = \tilde{\mathbf{x}}_k - \sum_{j=1}^{q} \theta_j \tilde{\mathbf{x}}_{k-j} \tag{24}$$

Clearly, if μ is a constant vector known in advance, we can estimate $\tilde{\mathbf{x}}_1, \tilde{\mathbf{x}}_2, \cdots, \tilde{\mathbf{x}}_t$ iteratively by minimizing $\|\tilde{\mathbf{x}}_k\|_1$ subject to (24) and $A_{k-i}\mathbf{x}_{k-i} = \mathbf{b}_{k-i}$ $(i = 0, 1, \cdots, p)$. If μ is unknown, we can impose the following constraints on μ

$$\mu = \frac{1}{t}\sum_{i=1}^{t} \mathbf{x}_i \tag{25}$$

$$\mathbf{b}_i = A_i\mathbf{x}_i, \qquad i = 0, 1, \cdots, t \tag{26}$$

We can then estimate each $\tilde{\mathbf{x}}_k$ by solving

$$\text{minimize } \|\tilde{\mathbf{x}}_k\|_1 \quad \text{subject to (24), (25) and (26).} \tag{27}$$

Note that the above ℓ^1 norm minimization problem involves constraints at all t time intervals. Although we can apply the techniques in Section 4.3 to reduce the problem size, the simplified problem can still be more expensive to solve than the case for ARIMA models with $d \geq 1$. A second limitation is that the algorithm can only be used for offline analysis, because μ depends on future time intervals.

There are many possible ways to alleviate the above limitations. For example, one can redefine μ as the mean of $\mathbf{x}_i$ within a small fixed time window observed in the past. Alternatively, one can define μ on a sliding window, *i.e.,* define $\mu_k = \frac{1}{w}\sum_{i=1}^{w} \mathbf{x}_{k-i}$, where w is the width of the sliding window. Note that the use of a sliding window effectively makes $d \geq 1$, because the AR polynomial $\Phi(L)$ is now

$$\Phi(L) = \left(1 - \sum_{i=1}^{p} \phi_i L^i\right)\left(1 - \frac{1}{w}\sum_{j=1}^{w} L^j\right),$$

which has a unit root $L = 1$. We will not further explore these possibilities in this paper, because we find that we need $d \geq 1$ on all our datasets as determined by our model selection procedure (described in Section 4.5.3).

4.5 Model selection and parameter estimation

In this section, we address two important issues on applying ARIMA type models: model selection (*i.e.,* determining p, d, q) and parameter estimation (*i.e.,* determining coefficients ϕ_i, θ_j). We do so by answering the following three questions.

4.5.1 What data to use?

The first question is what data to use for model selection and parameter estimation. This is important because the data determines the model and the parameters that we can learn.

In the context of network anomography, we would like the model and parameters to capture the normal behavior of $\mathbf{x}_i$. For this purpose, we propose to select our models and parameters based on the traffic aggregated at different *ingress* points. More specifically, let I be the set of indices corresponding to all the ingress points in the link load vectors $\mathbf{b}_i$. We will use the series of subvectors $\mathbf{b}_i^I$ as the input data for model selection and parameter estimation.

This has several advantages. First, $\mathbf{b}_i^I$ is readily available and does not require any inference. More importantly, ingress traffic is largely invariant to internal topology and routing changes in the local domain under consideration, making our algorithms applicable even in the presence of topology and routing changes. In addition, each element of $\mathbf{b}_i^I$ aggregates a number of OD flows. So the effect of anomalies or missing data on individual OD flows is less significant, making our results more robust.

4.5.2 How to estimate ϕ_i and θ_j given (p, d, q)?

Given (p, d, q) and input vector series $\{\mathbf{b}_k^I\}$, we can estimate the autoregression and moving-average coefficients ϕ_i and θ_j by constructing a state-space model and then applying the standard Kalman filter adaptation [18, 25]. Our implementation is based on the `armax` function in Matlab's System Identification Toolbox [25].

To ensure the size of the resulting state-space model is acceptable by Matlab, we currently estimate ϕ_i and θ_j based on the 10 rows with the highest row sums in matrix $[\mathbf{b}_1^I\mathbf{b}_2^I\cdots\mathbf{b}_t^I]$. We have also experimented with an alternative scheme that partitions all the rows of $[\mathbf{b}_1^I\mathbf{b}_2^I\cdots\mathbf{b}_t^I]$ into 10 groups and estimates the parameters from the 10 aggregated traffic series (one per group). We find that the estimated coefficients are similar under the two schemes.

4.5.3 How to select the model order (p, d, q)?

We first select the degree of differencing (d). As noted in [28, Lecture 9], the optimal degree of differencing is often the one at which the standard deviation of the differenced series is the lowest. We can apply this rule to determine d. More specifically, for each $d \in \{0, 1, 2, 3, 4\}$, we compute the differenced series

$$Z_d = [\mathbf{z}_{d,1}\mathbf{z}_{d,2}\cdots\mathbf{z}_{d,t}] = (1 - L)^d[\mathbf{b}_1^I\mathbf{b}_2^I\cdots\mathbf{b}_t^I]$$

Let $E[Z_d] = \frac{1}{t}\sum_{i=1}^{t}\mathbf{z}_{d,i}$ and $V[Z_d] = \frac{1}{t}\sum_{i=1}^{t}\|\mathbf{z}_{d,i} - E[Z_d]\|_2^2$. We then pick the d that results in the minimum variance $V[Z_d]$. In all the datasets we tested in this paper, we find that we need $d = 1$.

Once we have d, we can automate the choice of p and q by applying an information based criterion such as the AIC or AICC (see [4, pp. 171–174]). Information based criteria are designed to achieve a good balance between model parsimony and low prediction error. In our Matlab implementation, we use AIC (Akaike's Information Criterion) as our model selection criterion. For each $p, q \in \{0, 1, 2, 3, 4\}$, we estimate ϕ_i and θ_j (as in Section 4.5.2) and compute the resulting AIC based on the residuals and the model complexity. We then choose the pair of (p, q) with the lowest AIC.

5. EVALUATION METHODOLOGY

5.1 Data Sets

We apply our techniques to real network measurement data gathered from two large backbone networks – Internet2's Abilene network and a Tier-1 ISP network. Both networks span the continental USA. However, the networks are very different in terms of number of nodes, traffic volume and traffic characteristics. The Abilene

backbone is relatively small, with 12 core routers, 15 backbone links and 144 OD flow elements in its traffic matrix[2]. In contrast, the Tier-1 ISP backbone is relatively large, consisting of hundreds of routers, thousands of links and tens of thousands of different OD flows. To reduce computation complexity without loss of utility, we use the technique in [39] to lump edge routers with topologically equivalent connectivity. This reduces the total number of OD flows to about 6000.

Another important distinction between the Abilene and the Tier-1 ISP networks is in the traffic they carry. Abilene is usually quite lightly loaded. Abilene's traffic comes mainly from major academic institutions, a significant portion of which consists of traffic whose characteristics resemble bulk data transfer and network measurement traffic. On the other hand, the Tier-1 ISP network is moderately loaded, carrying primarily commercial traffic. On inspection of the traffic behavior, we found that the Abilene traffic exhibits irregularity and much higher variability than that of the Tier-1 ISP. These distinctions will impact the performance of the anomaly detection techniques explored here; in particular, anomalies stand out more strikingly in Abilene data.

The primary data inputs for our anomaly diagnosis are the time series of link loads (bytes across interfaces) for every network, gathered through SNMP. We use flow level data, where available, for validation. As is often the case, the flow data is incomplete. The flow data are collected at the edge of the network where data packets are sampled and aggregated by the IP source and destination address, and the TCP port number. Adjusted for sampling rate and combined with BGP and ISIS/OSPF routing information, these sampled IP flow statistics are then aggregated into a real traffic matrix [13], where each element is an OD flow with the origin and destination being the ingress and egress point of the flow to/from the network. Consistent with [23], we aggregate these measurements into bins of 10 minutes to avoid any synchronization issues that could have arisen in the data collection.

Ideally, to evaluate the methods, one would like complete flow level data, SNMP link load measurements, and continuous tracking of routing information, providing a consistent, comprehensive view of the network in operation. Unfortunately, we do not have the complete set of flow level data across the edge of the network (due to problems in vendor implementations or in data collection), and our routing information is only "quasi-" real time (we rely on snapshots available from table dumps carried out every 8 hours). As a result, inconsistencies sometimes arise between these measurements. To overcome these problems and provide a consistent means for evaluating the algorithms, we adopt the method in [39] and reconstruct the link traffic data by simulating the network routing on the OD flow traffic matrix generated from the available set of flow level data. Note that we use derived link load measurements for validation purposes only. In practice, our methods are applicable to direct measurement of traffic data as obtained from SNMP.

5.2 Performance Metrics

We conduct our evaluation in two steps. First, we compare the different solution techniques for the inverse problem $\tilde{\mathbf{b}}_j = A\tilde{\mathbf{x}}_j$ (as described in Section 3.4). The inverse problem is common to all the late-inverse anomography methods discussed in Section 3, so for simplicity we choose to use the simplest temporal forecasting model, ARIMA$(0,1,0)$, for evaluation. This model predicts the next observation to have the same value as the current one. Thus, the inverse problem on the prediction error can be constructed by simply taking the difference between consecutive link load observations: $A\tilde{\mathbf{x}}_t = \tilde{\mathbf{b}}_t = \mathbf{b}_t - \mathbf{b}_{t-1}$. The performance of the inversion technique is measured by comparing the inferred solution, $\tilde{\mathbf{x}}_t$, to the direct difference of the OD flow, $\mathbf{x}_t - \mathbf{x}_{t-1}$; the closer the values are, the better the result. In the context of anomaly detection, it is often the case that the large elements (large volume changes) are of chief interest to network management. Hence, we defined a metric – detection rate – to compare the top ranked N elements (sorted by size) in solution $\tilde{\mathbf{x}}_t$ to the top N prediction errors $\mathbf{x}_t - \mathbf{x}_{t-1}$ for t spanning a period of one week. As we will see in Section 6, the top anomalies in our data are easily resolved by magnitude (close ties are rare). The *detection rate* is the ratio of the overlap between the two sets. Note that the detection rate avoids some problems with comparing false-alarm versus detection probabilities, as it combines both into one measure. A high detection rate indicates good performance. Detection rate is used to compare inference techniques in Section 6.1, to assess sensitivity to λ, and robustness to noise in Section 6.2, and the effectiveness of the methods for time-varying routing in Section 6.3.

In Section 6.4.2 we step away from the simple anomaly detection algorithm applied to test the inference component, and compare the complete set of anomography methods described in Section 3. As before we use detection rate to measure whether the anomaly detection method produces similar results when applied to the OD pairs directly, or applied to the link load data, along with an inversion method — we use the Sparsity-L1 method (the best performing of the methods tested using the methodology above). In other words, we benchmark the anomography method against the anomalies seen in direct analysis of the OD flows.

Since different methods may find different sets of benchmark anomalies, we need an objective measure for assessing the performance of the methods. Ideally, we would like to compare the set of anomalies identified by each of the methods to the set of "true" network anomalies. However, isolating and verifying all genuine anomalies in an operational network is, although important, a very difficult task. It involves correlating traffic changes with other data sources (e.g., BGP/OSPF routing events, network alarms, and operator logs), an activity that often involves case-by-case analysis. Instead, we perform pair-wise comparisons, based on the top ranked anomalies identified by each of the anomography methods, an approach also taken in Lakhina *et al.* [23].

Specifically, for each of the anomography methods, we apply the underlying anomaly detection method directly to the OD flow data. We think of the top ranked M anomalies, denoted by the set $\mathcal{B}_M^{(j)}$ for anomaly detection method j as a benchmark. For each of the anomography methods i, we examine the set of N largest anomalies $\mathcal{A}_N^{(i)}$ inferred from link load data. To help understand the fidelity of the anomography methods we consider the overlap between the benchmark and the anomography method, $\mathcal{A}_N^{(i)} \cap \mathcal{B}_M^{(j)}$, across the benchmarks and the anomography methods. We allow a small amount of slack (within one ten-minute time shift) in the comparison between events, in order that phase differences between methods not unduly impact the results.

We are interested in understanding both false positives and false negatives:

(i) False Positives. Taking $\mathcal{B}_M^{(j)}$ as the benchmark, the false positives produced by anomography method i are $\mathcal{A}_N^{(i)} - \mathcal{B}_M^{(j)}$. The magnitudes of the anomalies in $\mathcal{A}_N^{(i)}$ and $\mathcal{B}_M^{(j)}$ may vary.

[2]The Abilene network studied in [23] was prior to some major network updates in 2003. For comparison purpose, we have included the same dataset, which has 11 core routers in the topology, hence 121 OD flows in the traffic matrix. We will refer to this dataset as Abilene*.

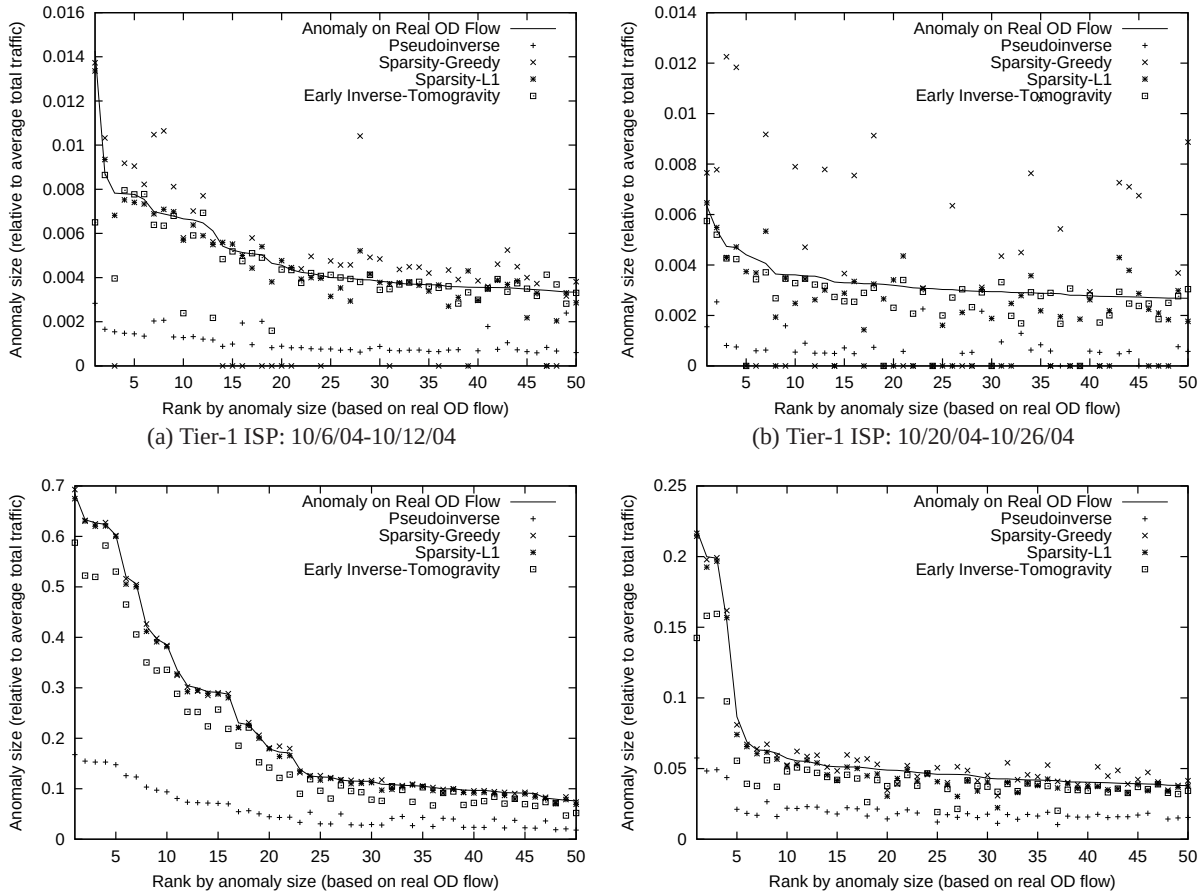

(a) Tier-1 ISP: 10/6/04-10/12/04

(b) Tier-1 ISP: 10/20/04-10/26/04

(c) Abilene: 6/26/04-7/2/04

(d) Abilene: 7/10/04-7/16/04

Figure 1: Anomalies by size

Yet, intuitively if one of the $N = 30$ top anomalies in $\mathcal{A}_N^{(i)}$ is not among the top $M = 50$ from the benchmark, then this anomaly in $\mathcal{A}_N^{(i)}$ is likely a false positive. This leads to the following heuristic for detecting false positives. We choose (reasonable) parameters N and M, with $N < M$, and count the false positives as the size of $\mathcal{A}_N^{(i)} - \mathcal{B}_M^{(j)}$.

(ii) False Negatives. Our reasoning is similar. Taking $\mathcal{B}_M^{(j)}$ as the benchmark, the false negatives produced by anomography method i are $\mathcal{B}_M^{(j)} - \mathcal{A}_N^{(i)}$. Intuitively if one of the $M = 30$ top anomalies in the benchmark is not among the top $N = 50$ anomalies in $\mathcal{A}_N^{(i)}$ then this anomaly in $\mathcal{B}_M^{(j)}$ is missed by the anomography method i, and is a false negative. This leads to the following heuristic for detecting false negatives. We choose (reasonable) parameters N and M, with $N > M$, and count the false negatives as the size of $\mathcal{B}_M^{(j)} - \mathcal{A}_N^{(i)}$.

For our reports in the next section, we choose the smaller of M and N to be 30, since this roughly represents the number of traffic anomalies that network engineers might have the resources to analyze deeply on a weekly basis. We would like to show comparative results where the larger parameter varies, but cannot within a reasonable amount of space, and so show results for one fixed value 50. It is important to note that the results we obtained for other values of M and N change none of our qualitative conclusions.

6. RESULTS

We obtained six months (03/01/04-09/04/04) of measurements for the Abilene network and one month (10/06/04-11/02/04) for the Tier-1 ISP network. We partitioned the data into sets spanning one week each, and evaluated the methods on each data set. Due to space limits, we present only a small set of representative results.

6.1 Comparison of Inference Techniques

We first compare different solution techniques for the inference problem $\tilde{\mathbf{b}} = A\tilde{\mathbf{x}}$. More specifically, we consider three late inverse algorithms: **Pseudoinverse** (Section 3.4.1), **Sparsity-Greedy** (Section 3.4.2.2), and **Sparsity-L1** (Section 3.4.2.1), and one early inverse technique: **Early Inverse-Tomogravity**. We choose to use the tomogravity method [40] as the early inverse technique since it has demonstrated high accuracy and robustness for estimating traffic matrix for real operational networks [16, 40].

Figure 1 (a) plots the sizes of the top 50 anomalies (the forecast errors) of the OD flows (the solid lines) and the corresponding values diagnosed by the different inference techniques (the points) for 10/6/04 to 10/12/04, for the Tier-1 ISP network. The y-axis provides the size of the anomalies normalized by the average total traffic volume on the network. The x-axis is the rank by the size of anomalies directly computed from the OD flows. We observe that there are very few large changes – among more than 6 million elements ($\sim$ 6000 OD flows at 1007 data points), there is one instance where the size of anomaly is more than 1% of total traffic and there are 18 cases where the disturbances constitute more than

0.5% of total traffic. This agrees with our intuition on the sparsity of network anomalies.

We see that Pseudoinverse significantly underestimates the size of the anomalies. Intuitively, Pseudoinverse finds the least square solution which distributes the "energy" of the anomaly evenly to all candidate flows that may have contributed to the anomaly, under the link load constraint. This is directly opposed to the sparsity maximization philosophy. Among the sparsity maximization techniques, Sparsity-L1 performs the best. Sparsity-L1 always finds solutions close to the real anomalies. Sparsity-Greedy, in general, is more effective than Pseudoinverse, although it sometimes overestimates the size of anomalies. As a representative of the early inverse technique, Tomogravity also performs well. With few exceptions, tomogravity finds solutions that track the real OD flow anomalies. Intuitively, when a proportionality condition holds, i.e., when the size of the anomalies are proportional to the sizes of the OD flows, then early inverse methods work well. However, where the proportionality condition does not hold, the error can be significant.

Figure 1 (b) presents the result of another week: 10/20/04 to 10/26/04. Comparing to Figure 1 (a), this data set contains almost no significant anomalies. It is desirable here to avoid overestimating the size of anomalies, creating false alarms. We observe that in this case, Sparsity-L1 and Early Inverse-Tomogravity can still provide good solutions that are close to real anomalies, while Sparsity-Greedy often overestimates the size of anomalies, and Pseudoinverse again performs poorly in comparison to the other techniques.

Figure 1 (c) and (d) depict two data sets of the Abilene network. We first notice that the relative size of anomalies (changes in traffic volume) are much larger than that of the Tier-1 ISP network. As noted earlier, the traffic on the Abilene network is relatively light and dominated by irregular traffic resembling bulk data transfers. This should make anomaly detection easier – it would be hard to miss any anomalous traffic behavior of the scale seen in these data sets (with individual anomalies constituting as much as 70% of total traffic). Regarding the performance of the different inference techniques here, both sparsity maximization methods produce very good results, with (in large part) overlapping solutions. This makes sense since the small size of the network leads to a simple inversion problem with few competing solutions. The early inverse technique, Tomogravity, does not perform well since the proportionality condition noted above is unlikely to hold for such irregular traffic patterns.

In the rest of the paper, we will only present the results for the data sets in Figure 1 (a) and (c), since they contain more interesting traffic anomalies.

Figure 2 presents the detection rate for the different inference techniques on the two data sets. We observe that for the Tier-1 ISP network, Sparsity-L1 and Tomogravity, which have about 0.8 detection rate, significantly outperform other methods. For the Abilene network, all methods except Pseudoinverse, achieve a high (close to 1) detection rate. Again, this is due to Abilene's small network size and large anomalies in traffic volumes.

Due to space limits, we will consider only Sparsity-L1 and Tomogravity in the rest of the evaluation, as these method demonstrate the greatest performance and flexibility in dealing with problems such as missing data and routing changes.

6.2 Robustness

6.2.1 λ in Sparsity-L1

Sparsity-L1 involves a parameter λ in its formulation (Eq. 11). Figure 3 investigates the sensitivity to the parameter choice. Specifically, Figure 3 plots the detection rate of Sparsity-L1 for $\lambda = 0.1$, 0.01, 0.001, 0.0001 and 0.00001. All λ in this range achieve good performance for both the Tier-1 ISP and the Abilene network. This is reassuring, since it suggests that little training or parameter tuning is needed to match the method to a different network or traffic pattern.

6.2.2 Measurement Noise

Thus far, we have assumed perfect link load information for anomaly detection. However, in real networks, SNMP byte counts are collected from all routers across the network. Inevitably, measurement issues such as lack of time synchronization may introduce noise. In this subsection, we evaluate the impact of measurement noise by multiplying white noise terms $N(1, \sigma)$ with each element of the link load, and then using the result as input to our inference algorithms.

Figure 4 compares how well the methods perform with no noise, to how well they do with noise levels $\sigma = 0.5\%$ and $\sigma = 1\%$. Note that measurement errors near 1% throughout the network are quite significant, since the size of the largest anomalies are themselves near 1% of the total traffic (Figure 1). It is a challenging task to accurately diagnose anomalies given the comparable level of noise. Nevertheless, we find that both Sparsity-L1 and Tomogravity are quite robust to measurement noise. For the Tier-1 ISP network, the detection rate remains above 0.8 for big anomalies (small N) and above 0.7 for the top 50 anomalies. For the Abilene network, there is hardly any degradation on the detection rate with this level of noise (small in comparison with the anomalies). These results demonstrate the strength of our algorithms in dealing with imperfect measurements.

6.3 Time Varying Routing Matrices

6.3.1 Missing Data

Missing measurement data, arising from problems such as packet loss during data collection, is common in real networks. Indeed, this can be tricky to be deal with, since the loss of link load data has the effect of producing time varying routing matrices in the anomography formulation. Fortunately, as discussed in Section 4, our extended Sparsity-L1 algorithm is able to handle this situation.

In Figure 5, we report on the performance of the inference algorithms with up to 5% of the data missing – missing values are selected uniformly at random. We observe that both Sparsity-L1 and Tomogravity suffer only minor (almost negligible) performance impact, in terms of detection rate. The low sensitivity to missing data is an important feature of these methods, since it is critical for real implementation.

6.3.2 Routing Changes

In an operational network, the routing matrix is unlikely to remain unchanged over a few days. Hardware failures, engineering operations, maintenance and upgrades all may cause traffic to be rerouted on alternative paths. In this subsection, we evaluate the impact of routing changes on the performance of our algorithms. We introduce routing changes by simulating faults on internal links. Figure 6 presents results where we have randomly failed/repaired up to 3 links at each time instance. We observe that Sparsity-L1 is very robust to such a disturbance in the routing structure, while Tomogravity suffers significant performance impact. It appears that Tomogravity suffers here because errors in the (early) inference step, being computed from different routing matrices, add to become comparable to the anomalies themselves. This demonstrates another advantage of the late-inverse over the early-inverse

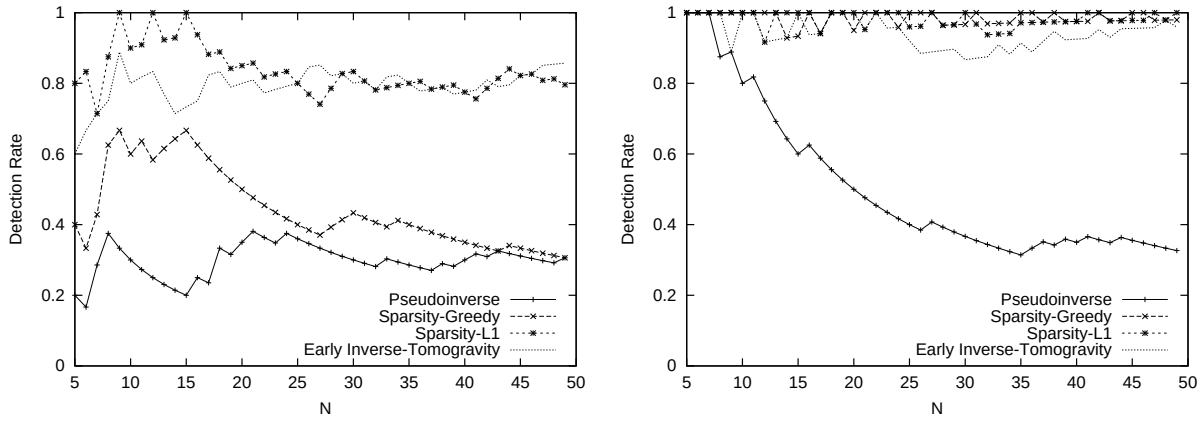

(a) Tier-1 ISP: 6/10/04-6/16/04 (b) Abilene: 6/26/04-7/2/04

Figure 2: Detection rate by various inference techniques

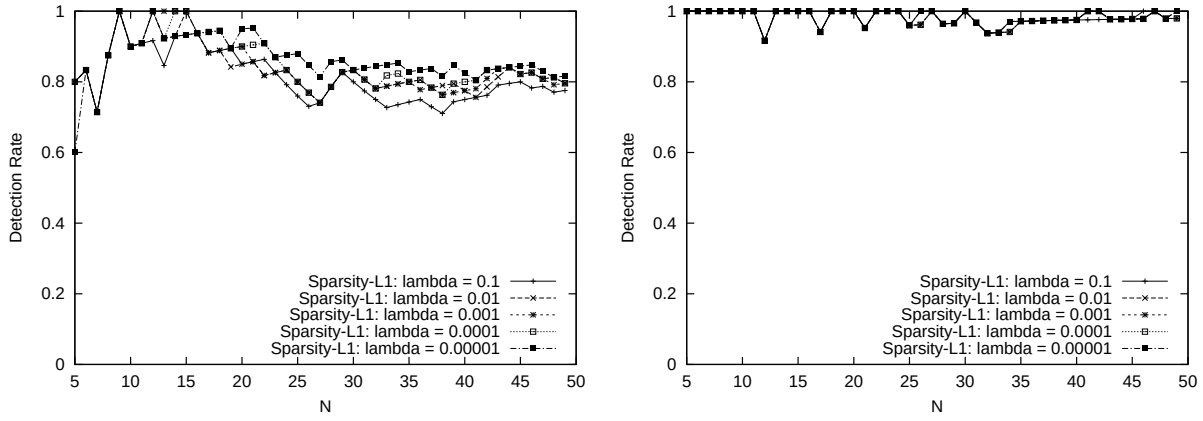

(a) Tier-1 ISP: 10/6/04-10/12/04 (b) Abilene: 6/26/04-7/2/04

Figure 3: Sensitivity to Parameter Choice: λ

approach.

6.4 Comparison of Anomography Methods

6.4.1 Impacts on Inference Accuracy

Thus far, we have compared the performance of Sparsity-L1 and Early Inverse-Tomogravity, under the simple temporal model (forecasting the next data point using the current value). We found that Sparsity-L1 in general outperforms the Early Inverse approach. The difference in performance is more pronounced for the Abilene network, where Tomogravity's underlying gravity modeling approach is challenged and the traffic pattern is highly variable. We also observed that Sparsity-L1 is robust to measurement noise, is insensitive to parameter choice, and is able to handle missing data and route changes. We now evaluate overall performance when applying Sparsity-L1 with other temporal and spatial anomography methods. In particular, we compare **FFT** (Section 3.3.2), **Wavelet** (Section 3.3.3), **PCA** (Section 3.2.1), **TPCA** (Section 3.3.4), and four ARIMA based methods, **Diff** (the simple forecasting model of the last section), **Holt-Winters**, **EWMA**, and general **ARIMA**, which determines the appropriate model using the method in Section 4.5.

As noted in Section 5, for each model considered, we compute $\tilde{\mathbf{x}}$ directly from the OD flow traffic data and use it as the benchmark. Next, we compute $\tilde{\mathbf{b}}$ with the same anomography model, and construct the $A\tilde{\mathbf{x}} = \tilde{\mathbf{b}}$ inference problem. We compare the solution derived through Sparsity-L1 with the benchmark. Figure 7 presents the detection rate for these approaches. To avoid overcrowding the graph, we divide the anomography methods into two groups. Figure 7 (a), (b) plot the results for the ARIMA family of anomography approaches and Figure 7 (c), (d) plot the results for the rest. We observe that for all the ARIMA based approaches, Sparsity-L1 finds very good solutions. With the traffic data aggregated at the 10-minute level, simple Diff and EWMA can sufficiently extract the anomalous traffic and warrant a solution that maximizes the sparsity of the anomalies. Holt-Winters produces better performance than Diff and EWMA. This is because the model is more sophisticated, and thus is able to capture more complex temporal trends exhibited in the traffic data. Further sophistication, as incorporated in ARIMA, however, cannot significantly improve performance. In the family of ARIMA models, Holt-Winters appears to provide the best complexity-performance trade-off.

From Figure 7 (c) and (d), we observe that Sparsity-L1 can also achieve high detection rate under FFT, Wavelet and TPCA. How-

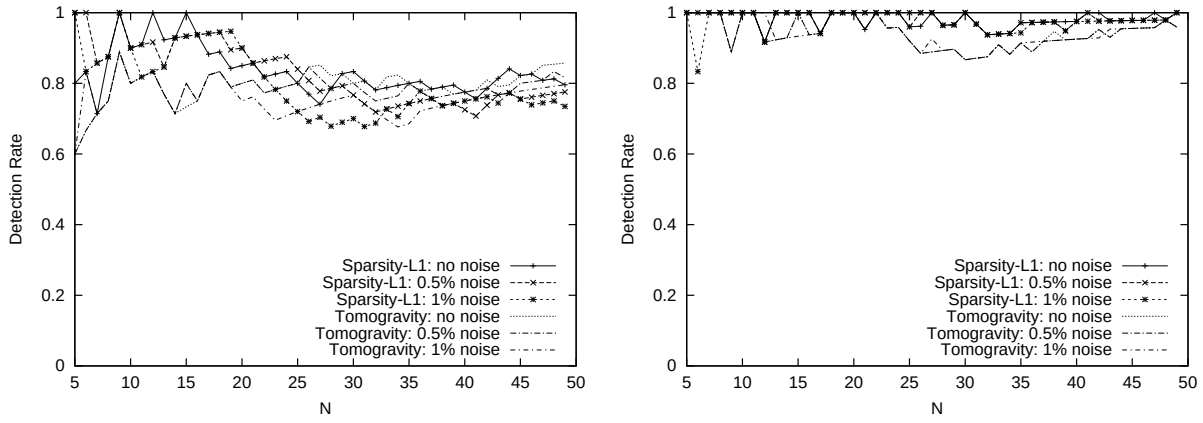

(a) Tier-1 ISP: 10/6/04-10/12/04 (b) Abilene: 6/26/04-7/2/04

Figure 4: Sensitivity to Measurement Noise

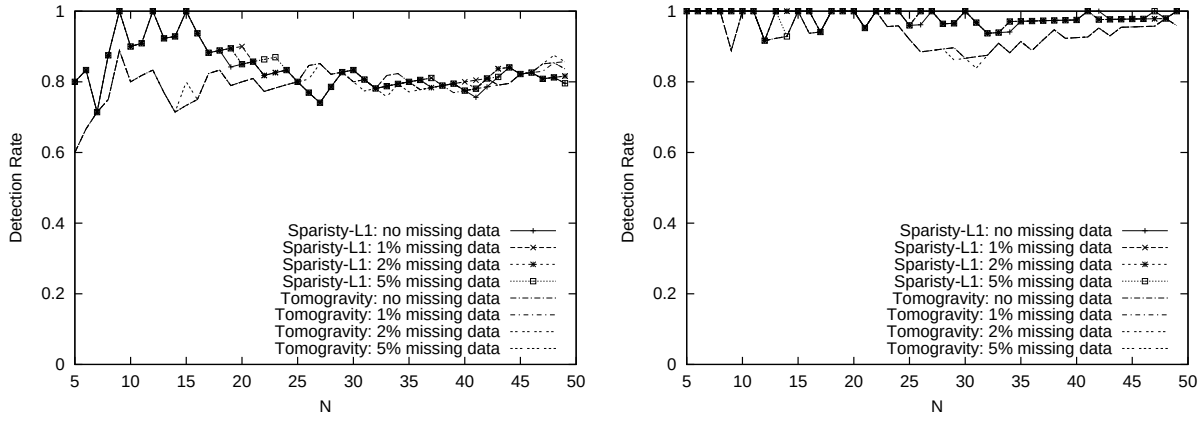

(a) Tier-1 ISP: 10/6/04-10/12/04 (b) Abilene: 6/26/04-7/2/04

Figure 5: Impact of Missing Data

ever, it doesn't work well with PCA[3]. This can be explained as follows. When we apply spatial PCA on the real traffic matrix X and the link load matrix B, we obtain two linear transformation $\tilde{X} = T_x X$, and $\tilde{B} = T_b B = T_b AX$, respectively. However, the two transformation matrices T_x and T_b may differ significantly because the spatial correlation among link loads and that among OD flows are rather different. Even if we use $T_x = T_b$, we cannot ensure that $AT_x X = T_b AX$ (i.e., $A\tilde{X} = \tilde{B}$ (Note that this last comment applies to spatial anomography methods in general). Thus, the spatial PCA anomography solution is not expected to completely overlap with the $\tilde{\mathbf{x}}$ identified by directly applying spatial PCA on the OD traffic flows. In contrast, the temporal anomography methods are *self-consistent* in that given $\tilde{B} = BT$, if we apply the same transformation T on X and obtain $\tilde{X} = XT$, we guarantee that $\tilde{B} = A\tilde{X}$ $(= AXT)$.

6.4.2 Cross Validation for Different Methods

We now turn to comparing the various anomography methods . To do so, we use a set of benchmarks, as described in Section 5, each derived from applying anomaly detection algorithm directly to the OD flows. For each benchmark, we report on the success of all of the anomography methods. The hope is that methods emerge that achieve both low false positives and low false negatives for nearly all of the benchmarks.

In Table 1 (a) we present the false positives for the Tier-1 ISP network with $M = 50$ and $N = 30$ (see Section 5). We found results for different values of M and N to be qualitatively quite similar. To align our results with the methodology reported in [23], we include the bottom row, labeled PCA*, where we use a squared prediction error (SPE) based scheme to determine the set of time intervals at which big anomalies occur, and the greedy approach (Section 3.4.2.2) to solve the inference problem. Note that the number of anomalies reported by PCA* may be less than N. We therefore report the actual number of anomalies in the table next to the label PCA*.

From the table, we observe from the upper left 6×6 quadrant that the ARIMA, FFT and Wavelet approaches tend to have relative low false positives among detected anomalies. Thus, the top 30 ranked anomalies derived through these approaches indeed appear to be anomalous traffic events that are worth investigating.

The PCA based approaches, however, exhibit a higher false positives when benchmarked against other approaches. This appears

[3]We have verified that Pseudoinverse and Sparsity-Greedy work even worse than Sparsity-L1 for PCA.

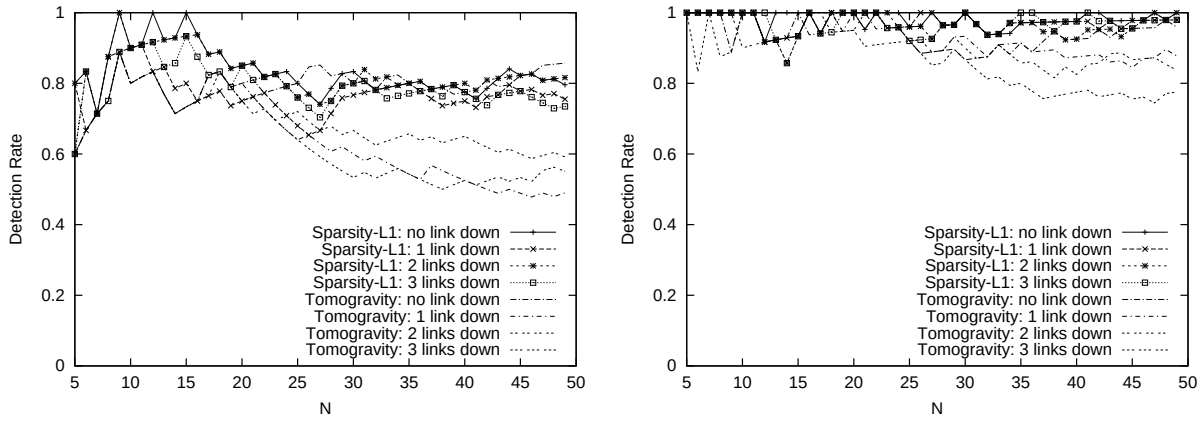

(a) Tier-1 ISP: 10/6/04-10/12/04

(b) Abilene: 6/26/04-7/2/04

Figure 6: Impact of Route Change

to be partially due to PCA identifying anomalies of a different type than those identified by the methods. Consider, for example, a sudden increase of traffic for an OD flow that persists for a couple of hours. PCA methods may identify every instance within the two-hour period as anomalous. ARIMA based approaches detect abrupt traffic changes. Hence ARIMA based methods likely extract only the "edges" – the first and last instance – of the two-hour period. Another factor contributing to PCA's false positives may be its lack of self-consistency: anomalies present in the OD pairs but not detected by the method in the link loads. In addition, unlike ARIMA, FFT, or wavelet based tomography, both spatial PCA and temporal PCA cannot fully utilize temporal ordering information in the measured time series data. For example, any reordering of the time series, $\mathbf{b}_1$, $\mathbf{b}_2$, ...,$\mathbf{b}_t$, does not affect the outcome of the algorithm.

Similar observations can be made from Table 1(b) and Table 1(c), where we present the same analysis, but for the Abilene network. In Table 1(b), we observe that PCA finds very few anomalies identified by other methods. Note that Table 1(c) uses the same dataset as that in [23], and the result is also consistent with that in [23].

Table 2 presents the number of false negatives for $M = 30$ and $N = 50$, where we are interested in the number of large anomalies that are not identified by each approach. We observe that the ARIMA methods, FFT and Wavelet anomography approaches have superb performance – the number of false negatives are very low for both the Tier-1 ISP network and the Abilene network. This indicates that very few important traffic anomalies can pass undetected by these approaches. The PCA based approaches, however, identify about half of the anomalies in the Tier-1 ISP network and almost none in Abilene. The high rate of false negatives for PCA in the Abilene network (Table 2 (b)) may be due to the high irregularity of the traffic pattern in this dataset – with anomalous traffic dominating the diurnal traffic variations. In such case, the normal subspace in PCA can be contaminated by the anomalous traffic, impacting the effectiveness of the method.

7. CONCLUSIONS

In this paper, we introduced *network anomography*, the problem of inferring network-level anomalies from widely available data aggregates. Our major advances are:

1. We introduced a powerful framework for anomography that cleanly separates the anomaly detection component from the inference component. The framework opens up a wide field for innovation and for the development of families of new algorithms. The novel method of Lakhina *et al.* based on PCA falls within the framework.

2. Within the framework, we put forward a number of novel algorithms, taking advantage of the range of choices for anomaly detection and inference components and choosing between temporal versus spatial approaches.

3. We developed a new *dynamic anomography* algorithm, which tracks both routing and traffic measurements, and so enables alerting with high fidelity on traffic matrix anomalies, without alerting on internal routing changes that leave the traffic matrix relatively stable. As routing changes are often due to normal internal self-healing behavior separating these changes from intrinsic traffic anomalies is advantageous. An additional benefit of dynamic anomography is that is robust to missing data, an important operational reality.

4. Using extensive data from Internet2's Abilene network and a Tier-1 ISP, we evaluated these anomography methods. The findings are encouraging. Specifically, the results indicate that the new set of *temporal* anomography methods introduced here have better fidelity, particularly when using l^1 minimization for the inference step. Dynamic anomography using ARIMA based methods and l^1 norm minimization shows uniformly high fidelity (low false positive and false negatives) and high robustness (to routing changes and missing or corrupted data).

While we believe our work represents a significant advance in the state of the art, we recognize that the the ultimate test of performance is significant operational experience: utility is bringing to light in the field new anomalies that were "flying under the radar" of other techniques, while producing very few false alarms. Our larger goal in future work is to explore the feasibility and performance of automated traffic management systems, which incorporate anomaly detection, root cause diagnosis and traffic and route control for operational networks.

8. REFERENCES

[1] P. Barford, J. Kline, D. Plonka, and A. Ron. A signal analysis of network traffic anomalies. In *Proc. ACM Internet Measurement Workshop*, November 2002.

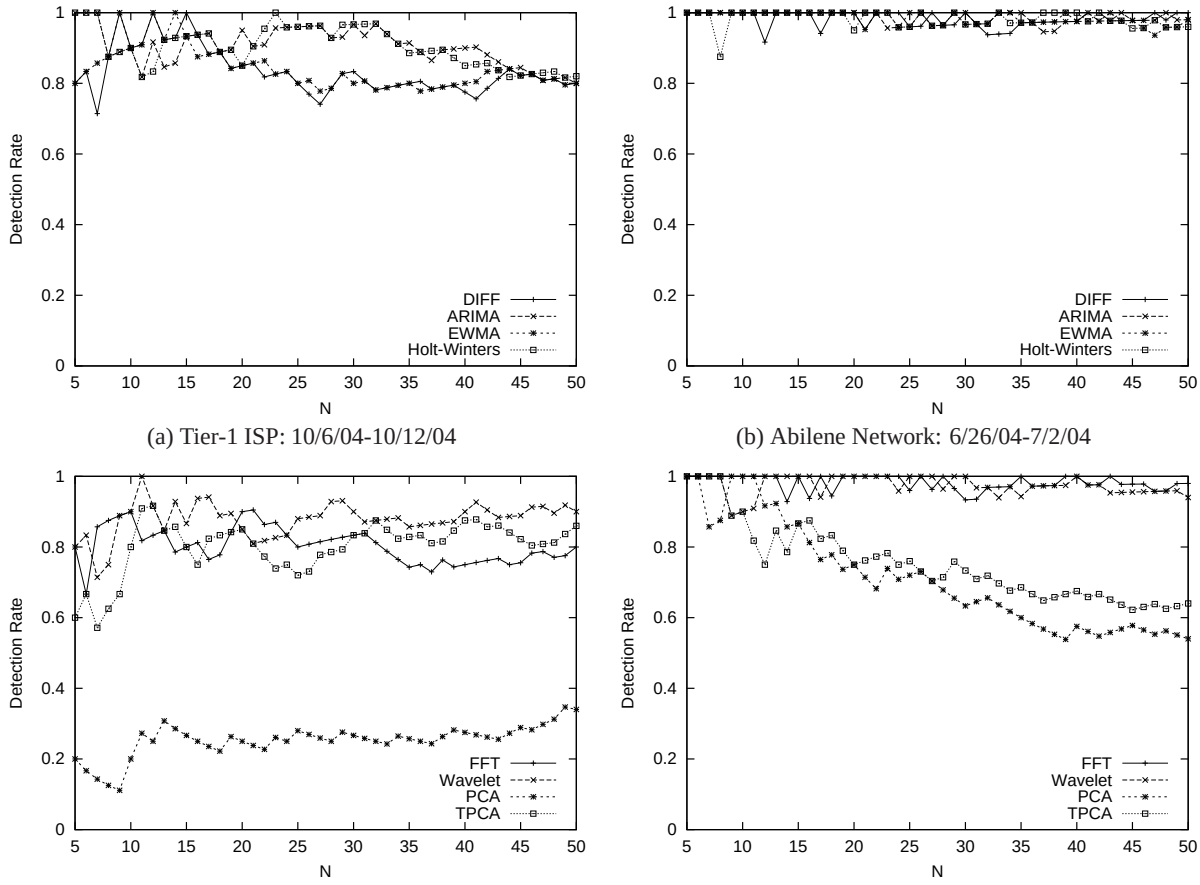

(a) Tier-1 ISP: 10/6/04-10/12/04

(b) Abilene Network: 6/26/04-7/2/04

(c) Tier-1 ISP: 10/6/04-10/12/04

(d) Abilene Network: 6/26/04-7/2/04

Figure 7: Sparsity-L1 under different anomography methods

[2] G. E. P. Box and G. M. Jenkins. *Time Series Analysis, Forecasting and Control*. Holden-Day, 1976.

[3] G. E. P. Box, G. M. Jenkins, and G. C. Reinsel. *Time Series Analysis, Forecasting and Control*. Prentice-Hall, Englewood Cliffs, 1994.

[4] P. J. Brockwell and R. A. Davis. *Introduction to Time Series and Forecasting*. Springer-Varlang, 2nd edition, 2002.

[5] J. D. Brutag. Aberrant behavior detection and control in time series for network monitoring. In *Proc. 14th Systems Administration Conference (LISA 2000)*, New Orleans, LA, USA, December 2000. USENIX.

[6] J. Cao, D. Davis, S. V. Wiel, and B. Yu. Time-varying network tomography. *J. Amer. Statist. Assoc*, 95(452):1063–1075, 2000.

[7] I. Daubechies. Orthonormal bases of compactly supported wavelets. *Communications on Pure and Applied Mathematics*, 41:909–996, 1988.

[8] I. Daubechies. *Ten Lectures on Wavelets*, volume 41 of CBMS-NSF Regional Conference Series in Applied Mathematics. SIAM, 1992.

[9] D. L. Donoho. For most large underdetermined systems of equations, the minimal l1-norm near-solution approximates the sparsest near-solution, August 2004. `http://www-stat.stanford.edu/~donoho/Reports/2004/l1l0approx.pdf`.

[10] D. L. Donoho. For most large underdetermined systems of equations, the minimal l1-norm solution is also the sparsest solution, September 2004. `http://www-stat.stanford.edu/~donoho/Reports/2004/l1l0EquivCorrected.pdf`.

[11] D. L. Donoho, M. Elad, and V. Temlyakov. Stable recovery of sparse overcomplete representations in the presence of noise, February 2004. `http://www-stat.stanford.edu/~donoho/Reports/2004/StableSparse-Donoho-etal.pdf`.

[12] A. Feldmann, A. Greenberg, C. Lund, N. Reingold, and J. Rexford. Netscope: Traffic engineering for IP networks. *IEEE Network Magazine*, pages 11–19, March/April 2000.

[13] A. Feldmann, A. G. Greenberg, C. Lund, N. Reingold, J. Rexford, and F. True. Deriving traffic demands for operational IP networks: methodology and experience. *IEEE/ACM ToN*, 2001.

[14] A. Graps. Amara's wavelet page, 2004. `http://www.amara.com/current/wavelet.html`.

[15] M. Grossglauser, N. Koudas, Y. Park, and A. Variot. Falcon: Fault management via alarm warehousing and mining. In *NRDM 2001 workshop*, Santa Barbara, CA, May 2001.

[16] A. Gunnar, M. Johansson, and T. Telkamp. Traffic matrix estimation on a large ip backbone: A comparison on real data. In *Proc. ACM Internet Measurement Conference*, October 2004.

[17] C. Hood and C. Ji. Proactive network fault detection. *IEEE Trans. Reliability*, 46(3):333–341, 1997.

[18] R. E. Kalman. A new approach to linear filtering and prediction problems. *Transactions of the ASME–Journal of Basic Engineering*, 82(Series D):35–45, 1960.

[19] L. A. Karlovitz. Construction of nearest points in the ℓ^p, p even and ℓ^1 norms. *Journal of Approximation Theory*, 3:123–127, 1970.

[20] Katzela and Schwartz. Schemes for fault identification in communication networks. *IEEE/ACM Transactions on Networking*, 3, 1995.

[21] B. Krishnamurthy, S. Sen, Y. Zhang, and Y. Chen. Sketch-based change detection: Methods, evaluation, and applications. In *ACM SIGCOMM Internet Measurement Conference*, Miami, FL, USA, October 2003.

[22] A. Lakhina, M. Crovella, and C. Diot. Characterization of

Top30 Inferred	False Positives with Top 50 Benchmark							
	Diff	ARIMA	EWMA	H-W	FFT	Wavelet	PCA	TPCA
Diff	**3**	**6**	**3**	**6**	**6**	**4**	14	14
ARIMA	**4**	**1**	**4**	**1**	**8**	**3**	10	13
EWMA	**3**	**6**	**3**	**6**	**7**	**5**	15	13
Holt-Winters	**4**	**1**	**4**	**1**	**8**	**3**	10	13
FFT	**6**	**6**	**6**	**7**	**2**	**6**	18	19
Wavelet	**6**	**6**	**6**	**6**	**8**	**1**	12	13
TPCA	17	17	17	17	20	13	14	0
PCA	18	18	18	18	20	14	14	1
PCA*(37)	18	17	18	17	23	16	11	8

(a) Tier-1 ISP

Top 30 Inferred	False Positives with Top 50 Benchmark							
	Diff	ARIMA	EWMA	H-W	FFT	Wavelet	PCA	TPCA
Diff	0	0	0	0	1	3	30	30
ARIMA	0	0	0	0	1	3	30	30
EWMA	0	0	0	0	2	2	30	30
Holt-Winters	0	0	0	0	2	2	30	30
FFT	2	2	1	1	0	0	30	30
Wavelet	3	3	1	1	0	0	30	30
TPCA	29	28	29	29	30	30	12	1
PCA	29	28	29	29	30	30	10	8
PCA*(26)	25	25	26	26	26	26	17	20

(b)Abilene

Top 30 Inferred	False Positives with Top 50 Benchmark							
	Diff	ARIMA	EWMA	H-W	FFT	Wavelet	PCA	TPCA
Diff	1	4	3	3	4	8	13	17
ARIMA	4	5	5	4	7	7	16	18
EWMA	4	5	5	4	7	7	16	18
Holt-Winters	3	5	4	2	7	8	15	17
FFT	9	10	10	10	3	10	17	18
Wavelet	10	8	10	10	9	2	19	18
TPCA	22	23	23	23	23	23	17	14
PCA	21	22	22	22	22	22	16	12
PCA*(19)	15	15	15	14	16	16	14	15

(c)Abilene*

Table 1: False positives seen in the top 30 inferred anomalies compared against the top 50 benchmark anomalies

Top 50 Inferred	False Negatives with Top 30 Benchmark							
	Diff	ARIMA	EWMA	H-W	FFT	Wavelet	PCA	TPCA
Diff	0	1	0	1	5	5	12	17
ARIMA	1	0	1	0	6	4	12	18
EWMA	0	1	0	1	5	5	12	17
Holt-Winters	1	0	1	0	6	4	12	18
FFT	3	8	4	8	1	7	18	19
Wavelet	0	2	1	2	5	0	11	13
TPCA	14	14	14	14	19	15	15	3
PCA	10	13	10	13	15	11	13	1
PCA*(37)	17	18	18	18	21	19	16	8

(a) Tier-1 ISP

Top 50 Inferred	False Negatives with Top 30 Benchmark							
	Diff	ARIMA	EWMA	H-W	FFT	Wavelet	PCA	TPCA
Diff	0	0	0	0	2	3	29	29
ARIMA	0	0	0	0	2	3	28	28
EWMA	0	0	0	0	2	2	28	28
Holt-Winters	0	0	0	0	2	2	28	28
FFT	1	1	1	1	0	0	29	29
Wavelet	1	1	1	1	0	0	30	30
TPCA	30	30	30	30	30	30	8	6
PCA	30	30	30	30	30	30	5	8
PCA*(26)	30	30	30	30	30	30	21	21

(b) Abilene

Top 50 Inferred	False Negatives with Top 30 Benchmark							
	Diff	ARIMA	EWMA	H-W	FFT	Wavelet	PCA	TPCA
Diff	3	5	5	4	8	8	15	19
ARIMA	2	3	4	3	8	8	16	19
EWMA	2	3	4	3	10	8	16	19
Holt-Winters	3	3	4	3	9	8	15	19
FFT	7	9	11	10	5	11	17	21
Wavelet	7	8	8	9	11	2	17	19
TPCA	21	23	23	22	23	23	19	14
PCA	18	20	21	20	23	22	18	14
PCA*(19)	27	27	27	27	28	27	25	24

(c) Abilene*

Table 2: False negatives seen in the top 50 inferred anomalies compared against the top 30 benchmark anomalies

network-wide anomalies in traffic flows. In *ACM SIGCOMM Internet Measurement Conference*, Taormina, Sicily, Italy, October 2004.

[23] A. Lakhina, M. Crovella, and C. Diot. Diagnosing network-wide traffic anomalies. In *Proc. ACM SIGCOMM 2004*, August 2004.

[24] A. Lakhina, K. Papagiannaki, C. D. Mark Crovella, E. D. Kolaczyk, and N. Taft. Structural analysis of network traffic flows. In *ACM SIGMETRICS / Performance*, 2004.

[25] L. Ljung. System identification toolbox user's guide (version 6). `http://www.mathworks.com/access/helpdesk/help/pdf_doc/ident/ident.pdf`.

[26] S. Mallat. *A Wavelet Tour of Signal Processing*. Academic Press, San Diego, 2nd edition, 2001.

[27] A. Medina, N. Taft, K. Salamatian, S. Bhattacharyya, and C. Diot. Traffic matrix estimation: Existing techniques and new directions. In *ACM SIGCOMM*, Pittsburg, USA, August 2002.

[28] R. F. Nau. Fuqua School of Business—Forecasting (course outline and lecture notes), 2003. `http://www.duke.edu/~rnau/411out03.html`.

[29] A. Nucci, R. Cruz, N. Taft, and C. Diot. Design of IGP link weights for estimation of traffic matrices. In *IEEE Infocom*, 2004.

[30] Y. C. Pati, R. Rezaiifar, and P. S. Krishnaprasad. Orthogonal matching pursuit: Recursive function approximation with applications to wavelet decomposition. In *Proc. 27th Annual Asilomar Conference on Signals, Systems, and Computers*, 1993.

[31] M. Roughan, T. Griffin, M. Mao, A. Greenberg, and B. Freeman. IP forwarding anomalies and improving their detection using multiple data sources. In *ACM SIGCOMM Workshop on Network Troubleshooting*, pages 307–312, Portland, OR, September 2004.

[32] SAS 9 online document. Equations for the smoothing models, Jan 2004.

[33] A. Shaikh, C. Isett, A. Greenberg, M. Roughan, and J. Gottlieb. A case study of OSPF behavior in a large enterprise network. In *ACM SIGCOMM Internet Measurement Workshop*, Marseille, France, 2002.

[34] C. Tebaldi and M. West. Bayesian inference on network traffic using link count data. *J. Amer. Statist. Assoc*, 93(442):557–576, 1998.

[35] R. Teixeira, N. Duffield, J. Rexford, and M. Roughan. Traffic matrix reloaded: Impact of routing changes renata teixeira. In *to appear in the Workshop on Passive and Active Measurements (PAM)*, 2005.

[36] M. Thottan and C. Ji. Proactive anomaly detection using distributed intelligent agents. *IEEE Network*, Sept/Oct 1998.

[37] Y. Vardi. Network tomography: estimating source-destination traffic intensities from link data. *J. Am. Statist. Assoc.*, 91:365–377, 1996.

[38] A. Ward, P. Glynn, and K. Richardson. Internet service performance failure detection. *ACM SIGMETRICS Performance Evaluation Review archive*, 26(3):38–43, December 1998.

[39] Y. Zhang, M. Roughan, N. Duffield, and A. Greenberg. Fast accurate computation of large-scale ip traffic matrices from link loads. In *Proc. ACM SIGMETRICS 2003*, June 2003.

[40] Y. Zhang, M. Roughan, C. Lund, and D. Donoho. An information-theoretic approach to traffic matrix estimation. In *Proc. ACM SIGCOMM*, August 2003.